Algebraic description of triaxially deformed rotational bands in odd mass nuclei

Kosai Tanabe[1] and Kazuko Sugawara-Tanabe[2]
[1]*Department of Physics, Saitama University, Sakura-Ku, Saitama 338-8570, Japan*
[2]*Otsuma Women's University, Tama, Tokyo 206-8540, Japan*
(Received 5 October 2005; published 9 March 2006)

An extensive application of the Holstein-Primakoff boson expansion to both single-particle angular momentum and total angular momentum provides an algebraic solution, which gives a good approximation to the exact results for the particle-rotor model with one high-j nucleon coupled to a triaxially deformed core. Two kinds of quantum numbers classify the rotational bands characteristic of the particle-rotor model and lead the selection rules for the interband and intraband transitions. The algebraic solution is compared with the experimental data for the odd mass isotopes ^{163,165,167}Lu as testing grounds.

DOI: 10.1103/PhysRevC.73.034305 PACS number(s): 21.10.Re, 21.60.Ev, 27.70.+q

I. INTRODUCTION

Recently, triaxial strongly deformed (TSD) bands have been observed in odd-A Lu isotopes ^{163}Lu [1–4], ^{165}Lu [5], and ^{167}Lu [6], which are interpreted as the wobbling excitations [7] based on the particle-rotor model with hydrodynamical moments of inertia [8,9]. It implies the applicability of the particle-rotor model with one valence nucleon in a high-j orbital coupled to a triaxially deformed even-even core for the rotational bands in odd-A nuclei with stable triaxial deformation. We proposed the application of the Holstein-Primakoff (HP) transformation to the total angular momentum $\vec{I}$ in even nuclei 35 years ago [10]. This treatment differs from that of the wobbling modes by Bohr and Mottelson [7] mainly in the order of approximation. It is obvious that the rotational energy spectra cannot be correctly reproduced only by the lowest-order terms arising from the HP boson expansion of the rotor Hamiltonian in $\hat{n}/(2I)$, where $\hat{n}$ is the HP boson number operator. This is also related to partial violation of the basic symmetries, i.e., the D_2 and Bohr symmetry groups, characteristic of the original Hamiltonian and its eigenstates. As different physical states are realized depending on the choice of moments of inertia, strength of single-particle potential, and deformation parameters, we need a suitable set of quantum numbers to classify the rotational bands in association with dynamical symmetries characteristic of the particle-rotor model. In other words, it is desirable that the physical contents of the rotational bands can be directly characterized by quantum numbers rather than by indirect evidence such as the expectation values of angular momenta [8,9].

In the present paper, we extend the HP boson expansion method [10] to the case of odd-A nuclei by introducing two kinds of bosons for the total angular momentum $\vec{I}$ and the single-particle angular momentum $\vec{j}$. We take into account the invariance of the nuclear states under the Bohr symmetry group [11], which imposes the restriction on the quantum numbers. Thus we can identify the nature of each band referring to two kinds of quantum numbers that indicate the precessions of $\vec{I}$ and $\vec{j}$. In this scheme, both angular momenta interact on an equal footing, and the precession of the core angular momentum $\vec{R} = \vec{I} - \vec{j}$ correlates with that of $\vec{j}$. Such an interplay between two tops with $\vec{R}$ and $\vec{j}$ may be called the "top-on-top mechanism." The body-fixed components of $\vec{R}$ and $\vec{j}$ do not commute each other but do not interact, while those of $\vec{I}$ and $\vec{j}$ commute each other but interact through the Coriolis term in the rotor Hamiltonian. Thus we may regard $\vec{I}$ and $\vec{j}$ as well as $\vec{R}$ and $\vec{j}$ as a correlating pair of tops in the top-on-top mechanism.

In Sec. II, we apply the HP boson expansion method to the model Hamiltonian and clarify the reason why we have to take into account the whole effect coming from the next-to-leading order in $1/(2I)$ and $1/(2j)$, in addition to the leading one. In Sec. III, we derive an approximate algebraic formula for the total Hamiltonian by applying the boson Bogoliubov transformation. To clarify the meaning of quantum numbers, we discuss the special case in which the single-particle potential vanishes. An alternative convenient form of the boson Bogoliubov transformation is given in Appendix A, which yields the same results as in Sec. III. A complete list of some relevant quantities is given in Appendix B. In Sec. IV, the algebraic method is applied to the matrix elements of electromagnetic transition operators. The selection rules are derived from the approximate expressions of the matrix elements for the interband and intraband transitions. Some of the transformation coefficients relating the original HP boson Fock space to the other boson Fock space are listed in Appendix C for further discussion. In Sec. V, we compare the algebraic formula with the exact results of energy levels and electromagnetic transition rates. The theoretical results with the rigid-body model are shown to be in good agreement with the experimental data of the TSD bands in Lu isotopes, as the realistic examples. In Sec. VI, the paper is concluded.

II. FORMALISM

A. Particle-rotor model

We adopt the particle-rotor Hamiltonian given by

$$H = H_{\rm rot} + H_{\rm sp}, \tag{1}$$

with

$$H_{\rm rot} = \sum_{k=x,y,z} A_k (I_k - j_k)^2, \tag{2a}$$

$$H_{\rm sp} = \frac{V}{j(j+1)} \left[\cos\gamma \left(3j_z^2 - \vec{j}^2 \right) - \sqrt{3} \sin\gamma \left(j_x^2 - j_y^2 \right) \right], \tag{2b}$$

where $\vec{I}$ is the total angular momentum, $\vec{j}$ is the single-particle angular momentum, and $A_k = 1/(2\mathcal{J}_k)$ ($k = 1, 2, 3$ or x, y, z).

We study two models for the moments of inertia $\mathcal{J}_k$, the hydrodynamical model in Copenhagen convention [7],

$$\mathcal{J}_k^{\rm hyd} = \frac{4}{3}\mathcal{J}_0 \sin^2\left(\gamma - \frac{2}{3}\pi k\right), \tag{3a}$$

and the rigid-body model in Lund convention,

$$\mathcal{J}_k^{\rm rig} = \frac{\mathcal{J}_0}{1 + \left(\frac{5}{16\pi}\right)^{1/2}\beta_2}\left[1 - \left(\frac{5}{4\pi}\right)^{1/2}\beta_2 \cos\left(\gamma + \frac{2}{3}\pi k\right)\right], \tag{3b}$$

where β_2 and γ are the deformation parameters describing the ellipsoidal shape of the rotor. Note that the maximum moment of inertia is about the x axis and the relation $\mathcal{J}_x \geqslant \mathcal{J}_y \geqslant \mathcal{J}_z$ holds in the range of $0 \leqslant \gamma \leqslant \pi/3$ for $\mathcal{J}^{\rm hyd}$ and in $0 \leqslant \gamma \leqslant 2\pi/3$ for $\mathcal{J}^{\rm rig}$. We have chosen the sign convention of γ in $\mathcal{J}_k$ as we study the case in which both $\vec{j}$ and $\vec{I}$ are aligned along the x axis in both models of moments of inertia. The sign of γ in $H_{\rm sp}$ is chosen so that the oscillator strength is the largest in the x direction to be consistent with the largest $\mathcal{J}_x^{\rm rig}$. The factors in Eqs. (3a) and (3b) are chosen so that $\mathcal{J}_x^{\rm hyd} = \mathcal{J}_x^{\rm rig} = \mathcal{J}_0$ at $\gamma = 0^\circ$. It is remarked that a common value of the scaling factor $s = \mathcal{J}_0 V$ yields the same physical contents except an energy scale, as inferred from Eqs. (2a), (2b), (3a), and (3b).

B. Bohr symmetry

We pay special attention to the important symmetry properties of the nuclear Hamiltonian and the nuclear state. It is obvious that the particle-rotor Hamiltonian is invariant with respect to rotations through the angle π about each of the three principal axes, $\mathcal{R}_k(\pi) = \exp(-i\pi R_k)$ with $R_k = I_k - j_k$ ($k = 1, 2, 3$). These symmetry operations are comprised in the D_2 symmetry group, which has four representations labeled by (r_1, r_2, r_3), where r_k stands for an eigenvalue of $\mathcal{R}_k(\pi)$, and takes either of $+1$ or -1, and $r_1 r_2 r_3 = 1$ [7].

The labeling of the principal axes is arbitrary, and the effect of an operation that relabels three axes can be compensated for by a proper change of deformation parameters (β_2, γ) if the nuclear deformation is of an ellipsoidal shape. These operations, each of which leaves a nuclear state invariant, compose the Bohr symmetry group (or the octahedral group O) [7,11]. Now we consider the effect of two elements from 24 group elements, i.e., $\mathcal{R}_2(\pi/2)$ and $\mathcal{R}_3(\pi/2)$ representing rotations through the angle $\pi/2$ about the intrinsic second and third axes, respectively:

$$\mathcal{R}_2(\pi/2)(\beta_2, \gamma, I_1, I_2, I_3)\mathcal{R}_2^\dagger(\pi/2) = (\beta_2, -\gamma + 2\pi/3, I_3, I_2, -I_1), \tag{4a}$$

$$\mathcal{R}_3(\pi/2)(\beta_2, \gamma, I_1, I_2, I_3)\mathcal{R}_3^\dagger(\pi/2) = (\beta_2, -\gamma, -I_2, I_1, I_3). \tag{4b}$$

Hence we find that twice the operations of each of these operators, i.e., $\mathcal{R}_2^2(\pi/2)$ and $\mathcal{R}_3^2(\pi/2)$, coincide with the D_2 operations $\mathcal{R}_2(\pi)$ and $\mathcal{R}_3(\pi)$ without changing deformation parameters (β_2, γ). Therefore Bohr symmetry requires that only the states belonging to $(r_1, r_2, r_3) = (+1, +1, +1)$ representation be allowed as nuclear states, unless the corresponding invariance of the Hamiltonian is violated for some reason. We refer to the invariance under both D_2 symmetry and Bohr symmetry simply as D_2 invariance hereafter.

Now we consider the case in which the x axis is chosen as a quantization axis. Then the physical states must be invariant under both operations $\mathcal{R}_3(\pi) = \exp[-i\pi(I_z - j_z)]$ and $\mathcal{R}_1(\pi) = \exp[-i\pi(I_x - j_x)]$. By multiplying a projection operator

$$\mathcal{P} = \tfrac{1}{4}[1 + \mathcal{R}_3(\pi)][1 + \mathcal{R}_1(\pi)] \tag{5}$$

on the state vector $|IK'\rangle|j\Omega'\rangle$ defined in the body-fixed frame, we construct a D_2-invariant state as

$$\sqrt{2}\mathcal{P}|IK'\rangle|j\Omega'\rangle = \frac{1 + (-1)^{K'-\Omega'}}{2\sqrt{2}}[|IK'\rangle|j\Omega'\rangle + (-1)^{I-j}|I - K'\rangle|j - \Omega'\rangle], \tag{6}$$

where K' and Ω' denote an eigenvalue of I_x and j_x, respectively. A numerical factor of $\sqrt{2}$ is introduced on the left-hand-side (l.h.s.) of Eq. (6) to normalize the projected state vector. Thus we find that a complete set of the D_2-invariant basis is provided by

$$\left\{\sqrt{\frac{2I+1}{16\pi^2}}\left[\mathcal{D}^I_{MK'}(\theta_i)\phi^j_{\Omega'} + (-1)^{I-j}\mathcal{D}^I_{M-K'}(\theta_i)\phi^j_{-\Omega'}\right];\ |K' - \Omega'| = \text{even},\quad \Omega' > 0\right\}, \tag{7}$$

where $\phi^j_{\Omega'}$ stands for spherical bases for the single-particle state, and $\mathcal{D}^I_{MK'}(\theta_i)$ is the Wigner $\mathcal{D}$ function. Since the magnitude R of the rotor angular momentum $\vec{R} = \vec{I} + (-\vec{j})$ is given by $R = |I - j|, |I - j| + 1, \ldots, I + j - 1$, or $I + j$, an integer $n_{\beta'}$ defined by $R = I - j + n_{\beta'}$ takes

$$n_{\beta'} = 0, 1, 2, \ldots, 2j - 1, \text{ or } 2j. \tag{8}$$

As R_x runs from R to $-R$ and $R_x = I_x - j_x = K' - \Omega' =$ even, an integer $n_{\alpha'}$ defined by the relation $R_x = R - n_{\alpha'}$ takes

$$\begin{aligned} n_{\alpha'} &= 0, 2, 4, \ldots, \text{or } 2R, && \text{for} \quad R = \text{even},\\ n_{\alpha'} &= 1, 3, 5, \ldots, \text{or } 2R - 1, && \text{for} \quad R = \text{odd}. \end{aligned} \tag{9}$$

Physical states are realized for a set of nonnegative integers $n_{\alpha'}$ and $n_{\beta'}$, which are related to the magnitude of rotor angular momentum R and its x component R_x through the relations $R = I - j + n_{\beta'}$ and $R_x = I - j + n_{\beta'} - n_{\alpha'}$ by the D_2 selection rule.

C. Holstein-Primakoff boson expansion method

It has been shown by the present authors [10] that the inclusion of higher-order terms in the HP boson expansion

is necessary for reproducing the rotational spectra of the triaxially deformed rotor of an even nucleus. In this section, we will see that this is also true for the odd-A nucleus in association with the D_2 invariance of the bosonized Hamiltonian. Here we extend the same method as given in Ref. [10] to the particle-rotor model by introducing two kinds of bosons for $\vec{I}$ and $\vec{j}$. Since the coefficient of I_x^2 and the coefficient of j_x^2 are the smallest among the other coefficients in Eqs. (2a) and (2b), it is expected that the total energy becomes lowest when both angular-momentum vectors $\vec{I}$ and $\vec{j}$ are aligned to the x direction. Therefore we choose diagonal forms for the components I_x and j_x in the HP boson representation as follows:

$$\begin{aligned} I_+ &= I_-^\dagger = I_y + iI_z = -\hat{a}^\dagger\sqrt{2I-\hat{n}_a}, \\ I_x &= I - \hat{n}_a \qquad \text{with} \quad \hat{n}_a = \hat{a}^\dagger\hat{a}; \end{aligned} \tag{10a}$$

$$\begin{aligned} j_+ &= j_-^\dagger = j_y + ij_z = \sqrt{2j-\hat{n}_b}\hat{b}, \\ j_x &= j - \hat{n}_b \qquad \text{with} \quad \hat{n}_b = \hat{b}^\dagger\hat{b}. \end{aligned} \tag{10b}$$

Using these representations, we rewrite Hamiltonian (1) in terms of two kinds of boson operators, $\hat{a}$ and $\hat{b}$.

As our purpose is to classify the rotational bands in terms of a set of quantum numbers, the D_2 invariance of the Hamiltonian is of central importance. Therefore it is interesting to know to what extent the D_2 invarinace of the Hamiltonian expressed in terms of HP bosons is maintained, depending on the level of approximation. Since I_x and j_x are diagonal in Eqs. (10), the effects of the transformation $\mathcal{R}_1(\pi)$ on $\hat{a}$ and $\hat{b}$ are expressed as $\mathcal{R}_1(\pi)\hat{a}\mathcal{R}_1^\dagger(\pi) = -\hat{a}$ and $\mathcal{R}_1(\pi)\hat{b}\mathcal{R}_1^\dagger(\pi) = -\hat{b}$. Therefore any product of an even number of $\hat{a}$, $\hat{b}$, $\hat{a}^\dagger$, and $\hat{b}^\dagger$ is invariant under the transformation $\mathcal{R}_1(\pi)$. The effects of the operator $\mathcal{R}_3(\pi)$ on $I_\pm$ and $j_\pm$ are expressed as

$$\mathcal{R}_3(\pi)I_\pm\mathcal{R}_3^\dagger(\pi) = -I_\mp,\ \mathcal{R}_3(\pi)j_\pm\mathcal{R}_3^\dagger(\pi) = -j_\mp. \tag{11}$$

In the following proof of the D_2 invariance, we expand the square roots $\sqrt{2I-\hat{n}_a}$ and $\sqrt{2j-\hat{n}_b}$ about arbitrary real numbers $2I_0(<2I)$ and $2j_0(<2j)$, regarding $(\hat{n}_a - 2I_0)/(2I-2I_0)$ and $(\hat{n}_b-2j_0)/(2j-2j_0)$ as small quantities:

$$\begin{aligned} \sqrt{2I-\hat{n}_a} &= \sqrt{2(I-I_0)-(\hat{n}_a-2I_0)} \\ &\cong \sqrt{2(I-I_0)}\left[1-\frac{\hat{n}_a-2I_0}{4(I-I_0)}\right], \\ \sqrt{2j-\hat{n}_b} &= \sqrt{2(j-j_0)-(\hat{n}_b-2j_0)} \\ &\cong \sqrt{2(j-j_0)}\left[1-\frac{\hat{n}_b-2j_0}{4(j-j_0)}\right]. \end{aligned} \tag{12}$$

Then the Hamiltonian contains the fourth-order terms in boson operators in addition to the second-order ones. For simplicity, we call this order of approximation "the second approximation," in contrast to "the first approximation." The latter includes only the lowest-order contributions from the expansion, and the Hamiltonian keeps only the second-order terms in boson operators.

At first, in applying the expansions to Eq. (1), four combinations that are originally D_2 invariant are approximated as

$$\begin{aligned} I_+I_- + I_-I_+ &\cong 2\big(I + 2I\hat{n}_a - \hat{n}_a^2\big), \\ I_+^2 + I_-^2 &\cong 2I\left(1-\frac{1}{4I}\right)\hat{a}^\dagger\hat{a}^\dagger - \hat{a}^\dagger\hat{a}^\dagger\hat{a}^\dagger\hat{a} + \text{H.c.}, \\ j_+j_- + j_-j_+ &\cong 2\big(j + 2j\hat{n}_b - \hat{n}_b^2\big), \\ j_+^2 + j_-^2 &\cong 2j\left(1-\frac{1}{4j}\right)\hat{b}^\dagger\hat{b}^\dagger - \hat{b}^\dagger\hat{b}^\dagger\hat{b}^\dagger\hat{b} + \text{H.c.} \end{aligned} \tag{13}$$

Not only are these expressions free from the constants I_0 and j_0, as pointed out in the appendix of Ref. [12], but also the final boson expressions for $I_+I_- + I_-I_+$ and $j_+j_- + j_-j_+$ coincide with exact ones that can be directly derived without any approximation. Thus a substantial improvement in the accuracy can be expected at the stage of the second approximation.

We convert the transformations in Eqs. (11) into the forms in the same order of approximation:

$$\begin{aligned} \mathcal{R}_3(\pi)\hat{a}^\dagger\left[1-\frac{\hat{n}_a-2I_0}{4(I-I_0)}\right]\mathcal{R}_3^\dagger(\pi) &\cong -\left[1-\frac{\hat{n}_a-2I_0}{4(I-I_0)}\right]\hat{a}, \\ \mathcal{R}_3(\pi)\hat{b}^\dagger\left[1-\frac{\hat{n}_b-2j_0}{4(j-j_0)}\right]\mathcal{R}_3^\dagger(\pi) &\cong -\left[1-\frac{\hat{n}_b-2j_0}{4(j-j_0)}\right]\hat{b}. \end{aligned} \tag{14}$$

The effect of the transformation generated by $\mathcal{R}_3(\pi)$ is nothing but an exchange between the first term and the second term in each combination, as is inferred from Eqs. (11). For example, an application of the first relation in Eqs. (12) converts $I_+I_- + I_-I_+$ into

$$\begin{aligned} 2(I-I_0)\Bigg\{&\hat{a}^\dagger\left[1-\frac{\hat{n}_a-2I_0}{4(I-I_0)}\right]\left[1-\frac{\hat{n}_a-2I_0}{4(I-I_0)}\right]\hat{a} \\ &+\left[1-\frac{\hat{n}_a-2I_0}{4(I-I_0)}\right]\hat{a}\hat{a}^\dagger\left[1-\frac{\hat{n}_a-2I_0}{4(I-I_0)}\right]\Bigg\}, \end{aligned} \tag{15}$$

which reduces to the right-hand-side (r.h.s.) of the first relation in relations (13). An operation of $\mathcal{R}_3(\pi)$ on expression (15) leads to exchange two terms because of the first relation in expressions (14) and its complex conjugate. Therefore an application of the approximate transformations in relations (14) to the r.h.s. of relations (13) leaves the operator expressions invariant. This implies that all the combinations in relations (13) are D_2 invariant consistently within the order of approximation, even in the first approximation. Similarly, the following combinations are expanded as

$$\begin{aligned} I_+j_- + I_-j_+ &\cong -2\sqrt{(I-I_0)(j-j_0)}\hat{a}^\dagger\hat{b}^\dagger \\ &\quad\times\left[1-\frac{\hat{n}_a-2I_0}{4(I-I_0)}-\frac{\hat{n}_b-2j_0}{4(j-j_0)}\right]+\text{H.c.}, \\ I_+j_+ + I_-j_- &\cong -2\sqrt{(I-I_0)(j-j_0)}\hat{a}^\dagger \\ &\quad\times\left[1-\frac{\hat{n}_a-2I_0}{4(I-I_0)}-\frac{\hat{n}_b-2j_0}{4(j-j_0)}\right]\hat{b}+\text{H.c.}, \end{aligned} \tag{16}$$

which depend on I_0 and j_0, but are D_2 invariant in each order of approximation.

Second, the following D_2-invariant combinations become exact in the second approximation:

$$I_x^2=(I-\hat{n}_a)^2,\ j_x^2=(j-\hat{n}_b)^2,\ I_x j_x=(I-\hat{n}_a)(j-\hat{n}_b). \quad (17)$$

The invariance of these expressions under the transformations

$$\mathcal{R}_3(\pi)I_x\mathcal{R}_3^\dagger(\pi)=-I_x,\ \mathcal{R}_3(\pi)j_x\mathcal{R}_3^\dagger(\pi)=-j_x, \quad (18)$$

or

$$\begin{aligned}\mathcal{R}_3(\pi)(I-\hat{n}_a)\mathcal{R}_3^\dagger(\pi)&=-(I-\hat{n}_a),\\ \mathcal{R}_3(\pi)(j-\hat{n}_b)\mathcal{R}_3^\dagger(\pi)&=-(j-\hat{n}_b),\end{aligned} \quad (19)$$

is evident. However, the first approximation yields expressions like

$$\begin{aligned}I_x^2&\cong(I-2I_0)^2-2(I-2I_0)(\hat{n}_a-2I_0),\\ j_x^2&\cong(j-2j_0)^2-2(j-2j_0)(\hat{n}_b-2j_0),\\ I_x j_x&\cong(I-2I_0)(j-2j_0)-(j-2j_0)(\hat{n}_a-2I_0)\\ &\quad-(I-2I_0)(\hat{n}_b-2j_0),\end{aligned} \quad (20)$$

which are not D_2 invariant for any choice of I_0 and j_0. Thus we have confirmed that an approximate D_2 invariance of the Hamiltonian is achieved in the second approximation. Since our interest is in the low-lying states, we put $2I_0=2j_0=0$ in subsequent sections.

III. ALGEBRAIC SOLUTION

Applying the HP transformation in Eqs. (10) to the Hamiltonian of Eq. (1), we expand $\sqrt{2I-\hat{n}_a}$ and $\sqrt{2j-\hat{n}_b}$ into series in $\hat{n}_a/(2I)$ and $\hat{n}_b/(2j)$ and retain up to the next-to-leading order. We arrive at an approximate Hamiltonian written in terms of two kinds of HP bosons:

$$H_B\cong H_0+H_2+H_4, \quad (21)$$

where H_0 denotes a constant that collects all the terms independently of the boson operators, H_2 are the bilinear forms of boson operators, and H_4 are the fourth-order terms. Their explicit forms are

$$\begin{aligned}H_0&=A_xI(I+1)-A_x(2Ij+I+j)+a_xj(j+1)\\ &\quad+\tfrac{1}{4}(A_{yzx}+a_{yzx})-V\cos\gamma,\end{aligned} \quad (22)$$

$$H_2=(\hat{a}^\dagger\quad\hat{b}^\dagger\quad\hat{a}\quad\hat{b})\begin{bmatrix}A&G&B&F\\ G&C&F&D\\ B&F&A&G\\ F&D&G&C\end{bmatrix}\begin{pmatrix}\hat{a}\\ \hat{b}\\ \hat{a}^\dagger\\ \hat{b}^\dagger\end{pmatrix}, \quad (23)$$

$$\begin{aligned}H_4&=-\frac{1}{2}A_{yzx}\hat{a}^\dagger\hat{a}^\dagger\hat{a}\hat{a}-\frac{1}{4}A_{yz}(\hat{a}^\dagger\hat{a}^\dagger\hat{a}^\dagger\hat{a}+\hat{a}^\dagger\hat{a}\hat{a}\hat{a})\\ &\quad-\frac{1}{2}a_{yzx}\hat{b}^\dagger\hat{b}^\dagger\hat{b}\hat{b}-\frac{1}{4}a_{yz}(\hat{b}^\dagger\hat{b}^\dagger\hat{b}^\dagger\hat{b}+\hat{b}^\dagger\hat{b}\hat{b}\hat{b})\\ &\quad-2A_x\hat{a}^\dagger\hat{a}\hat{b}^\dagger\hat{b}-\frac{1}{4}A_y\left\{\sqrt{\frac{j}{I}}(\hat{a}^\dagger\hat{a}^\dagger\hat{a}+\hat{a}^\dagger\hat{a}\hat{a})(\hat{b}^\dagger+\hat{b})\right.\\ &\quad\left.+\sqrt{\frac{I}{j}}(\hat{a}^\dagger+\hat{a})(\hat{b}^\dagger\hat{b}^\dagger\hat{b}+\hat{b}^\dagger\hat{b}\hat{b})\right\}\\ &\quad-\frac{1}{4}A_z\left\{\sqrt{\frac{j}{I}}(\hat{a}^\dagger\hat{a}^\dagger\hat{a}-\hat{a}^\dagger\hat{a}\hat{a})(\hat{b}^\dagger-\hat{b})\right.\\ &\quad\left.+\sqrt{\frac{I}{j}}(\hat{a}^\dagger-\hat{a})(\hat{b}^\dagger\hat{b}^\dagger\hat{b}-\hat{b}^\dagger\hat{b}\hat{b})\right\},\end{aligned} \quad (24)$$

where the coefficients are defined by

$$\begin{aligned}A_{yzx}&=A_y+A_z-2A_x,\quad A_{yz}=A_y-A_z,\\ a_x&=A_x-\frac{\sqrt{3}V\sin\gamma}{j(j+1)},\\ a_{yz}&=A_{yz}+\frac{\sqrt{3}V}{j(j+1)}(\sin\gamma-\sqrt{3}\cos\gamma),\\ a_{yzx}&=A_{yzx}+\frac{3V}{j(j+1)}(\cos\gamma+\sqrt{3}\sin\gamma),\\ A&=\frac{1}{2}\left(I-\frac{1}{2}\right)A_{yzx}+jA_x,\quad B=\frac{1}{2}\left(I-\frac{1}{4}\right)A_{yz},\\ C&=\frac{1}{2}\left(j-\frac{1}{2}\right)a_{yzx}+IA_x,\quad D=\frac{1}{2}\left(j-\frac{1}{4}\right)a_{yz},\\ F&=\frac{1}{2}\sqrt{Ij}(A_y+A_z),\quad G=\frac{1}{2}\sqrt{Ij}A_{yz}.\end{aligned} \quad (25)$$

The diagonalization of H_2 in Eq. (23) is attained by the unitary transformation (or the boson Bogoliubov transformation) connecting boson operators $(\hat{a},\hat{b},\hat{a}^\dagger,\hat{b}^\dagger)$ to quasiboson operators $(\alpha,\beta,\alpha^\dagger,\beta^\dagger)$, i.e.,

$$\begin{pmatrix}\hat{a}\\ \hat{b}\\ \hat{a}^\dagger\\ \hat{b}^\dagger\end{pmatrix}=\begin{bmatrix}u_+&w_+&u_-&w_-\\ v_+&t_+&v_-&t_-\\ u_-&w_-&u_+&w_+\\ v_-&t_-&v_+&t_+\end{bmatrix}\begin{pmatrix}\alpha\\ \beta\\ \alpha^\dagger\\ \beta^\dagger\end{pmatrix}. \quad (26)$$

To get eigenvalues and eigenfunctions, we solve the following eigenvalue equation:

$$\begin{aligned}&\begin{bmatrix}A&G&B&F\\ G&C&F&D\\ -B&-F&-A&-G\\ -F&-D&-G&-C\end{bmatrix}\begin{bmatrix}u_+&w_+&u_-&w_-\\ v_+&t_+&v_-&t_-\\ u_-&w_-&u_+&w_+\\ v_-&t_-&v_+&t_+\end{bmatrix}\\ &=\begin{bmatrix}u_+&w_+&u_-&w_-\\ v_+&t_+&v_-&t_-\\ u_-&w_-&u_+&w_+\\ v_-&t_-&v_+&t_+\end{bmatrix}\begin{bmatrix}\omega&0&0&0\\ 0&\omega&0&0\\ 0&0&-\omega&0\\ 0&0&0&-\omega\end{bmatrix}.\end{aligned} \quad (27)$$

Here we take into account a metric matrix arising from boson commutation relations, which give negative signs in front of the matrix elements in the third and fourth rows on both sides of the equation. We obtain two positive eigenvalues $\omega^{(\pm)}(\omega^{(+)}\geqslant\omega^{(-)}\geqslant 0)$ and corresponding normalized eigenvectors by solving a fourth-order algebraic equation of ω. Two positive eigenvalues $\omega^{(\pm)}$ are given by

$$\omega^{(\pm)}=\sqrt{\frac{1}{2}(a^2+b^2)+g^2-f^2\pm r}, \quad (28)$$

with

$$r = \sqrt{\left[\tfrac{1}{2}(a^2 - b^2)\right]^2 + g^2(a+b)^2 - f^2(a-b)^2}, \quad (29)$$

where a, b, f, and g are related to A, B, F, and G through

$$\begin{aligned} a &= \frac{A}{|A|}\sqrt{A^2 - B^2},\ b = \frac{C}{|C|}\sqrt{C^2 - D^2}, \\ f &= F(P_+Q_+ + P_-Q_-) + G(P_+Q_- + P_-Q_+), \\ g &= F(P_+Q_- + P_-Q_+) + G(P_+Q_+ + P_-Q_-), \end{aligned} \quad (30)$$

with

$$\begin{aligned} P_\pm &= -\frac{B}{|B|}\left[\frac{1}{2}\left(\frac{|A|}{\sqrt{A^2 - B^2}} \pm 1\right)\right]^{1/2} \\ Q_\pm &= -\frac{C}{|C|}\left[\frac{1}{2}\left(\frac{|C|}{\sqrt{C^2 - D^2}} \pm 1\right)\right]^{1/2}. \end{aligned} \quad (31)$$

Thus eight transformation coefficients are determined, and the normalized eigenvector belonging to the eigenvalue $\omega^{(+)}$ is provided by the array

$$\begin{aligned} u_+ &= U_+P_+ + U_-P_-, \\ v_+ &= V_+Q_+ + V_-Q_-, \\ u_- &= U_-P_+ + U_+P_-, \\ v_- &= V_-Q_+ + V_+Q_-, \end{aligned} \quad (32a)$$

and the one belonging to $\omega^{(-)}$ by the array

$$\begin{aligned} w_+ &= W_+P_+ + W_-P_-, \\ t_+ &= T_+Q_+ + T_-Q_-, \\ w_- &= W_-P_+ + W_+P_-, \\ t_- &= T_-Q_+ + T_+Q_-, \end{aligned} \quad (32b)$$

where the quantities $U_\pm$, $W_\pm$, $V_\pm$, and $T_\pm$ are defined by

$$\begin{aligned} U_\pm &= \pm N^{(+)}\begin{Bmatrix} f \\ g \end{Bmatrix}\left[\omega^{(+)}(a \mp b) + \frac{1}{2}(a \mp b)^2 + r\right] \\ &\quad \times\left[\pm\omega^{(+)}(a+b) + \frac{1}{2}(a+b)^2 + r\right], \\ V_\pm &= \pm 2afN^{(+)}\begin{Bmatrix} g \\ f \end{Bmatrix}\left[\omega^{(+)}(a \pm b) + \frac{1}{2}(a \pm b)^2 + r\right], \\ W_\pm &= \pm N^{(-)}\begin{Bmatrix} f \\ g \end{Bmatrix}\left[\omega^{(-)}(a \mp b) + \frac{1}{2}(a \mp b)^2 - r\right], \\ &\quad \times\left[\pm\omega^{(-)}(a+b) + \frac{1}{2}(a+b)^2 - r\right], \\ T_\pm &= \pm 2afN^{(-)}\begin{Bmatrix} g \\ f \end{Bmatrix}\left[\omega^{(-)}(a \pm b) + \frac{1}{2}(a \pm b)^2 - r\right], \end{aligned} \quad (33)$$

and the normalization factor is given by

$$\begin{aligned} [N^{(\pm)}]^{-2} &= -g^2\left[\omega^{(\pm)}(a+b) + \tfrac{1}{2}(a+b)^2 \pm r\right]^2 \\ &\quad \times\left\{\left[-\omega^{(\pm)}(a+b) + \tfrac{1}{2}(a+b)^2 \pm r\right]^2 - 4a^2f^2\right\} \\ &\quad + f^2\left[\omega^{(\pm)}(a-b) + \tfrac{1}{2}(a-b)^2 \pm r\right]^2 \\ &\quad \times\left\{\left[\omega^{(\pm)}(a+b) + \tfrac{1}{2}(a+b)^2 \pm r\right]^2 - 4a^2f^2\right\}. \end{aligned} \quad (34)$$

We can confirm that the four relations that are required by the unitarity of the transformation in Eq. (26) are satisfied, i.e.,

$$\begin{aligned} &u_+^2 - u_-^2 + w_+^2 - w_-^2 = v_+^2 - v_-^2 + t_+^2 - t_-^2 = 1, \\ &u_+v_- - u_-v_+ + w_+t_- - w_-t_+ \\ &\quad = u_+v_+ - u_-v_- + w_+t_+ - w_-t_- = 0. \end{aligned} \quad (35)$$

Another useful parametrization of the boson Bogoliubov transformation can be introduced by an extensive application of the Bloch-Messiah theorem [13], which is discussed in Appendix A. In the practice of numerical analysis, we examined our program by confirming that both methods give the same results.

Finally, H_2 is diagonalized as

$$H_2 \simeq 2\omega_\alpha(\hat{n}_\alpha + 1/2) + 2\omega_\beta(\hat{n}_\beta + 1/2), \quad (36)$$

where we introduce number operators in the new quasiparticle picture,

$$\hat{n}_\alpha = \alpha^\dagger\alpha, \quad \hat{n}_\beta = \beta^\dagger\beta. \quad (37)$$

Since there remains a freedom in giving the names of α and β to new quasiparticles, we need a formula for identifying the lower-energy eigenvalue $\omega^{(-)}$ with ω_α, or ω_β. The eigenvector in Eqs. (32b) stands for a transformation

$$\beta = w_+\hat{a} + t_+\hat{b} + w_-\hat{a}^\dagger + t_-\hat{b}^\dagger. \quad (38)$$

If $|t_+| > |w_+|$, we can determine that the new quasipaticle β (α) continues the character of the quasiparticle $\hat{b}$ ($\hat{a}$) mainly, and we put $\omega_\beta = \omega^{(-)}$ ($\omega_\alpha = \omega^{(+)}$). On the other hand, if $|t_+| < |w_+|$, we exchange α with β and put $\omega_\beta = \omega^{(+)}$($\omega_\alpha = \omega^{(-)}$).

To take account of higher-order contributions, we apply the boson transformation in Eq. (26) to H_4, defined by Eq. (24), and retain only diagonal terms that are expressed in terms of $\hat{n}_\alpha$ and $\hat{n}_\beta$. Note that this procedure is nothing but the first iteration and is equivalent to the first-order perturbation treatment. As a result we arrive at an approximate formula for H_4 as

$$H_4 \simeq C_0 + C_\alpha\hat{n}_\alpha + C_\beta\hat{n}_\beta + C_{\alpha\alpha}\hat{n}_\alpha^2 + C_{\beta\beta}\hat{n}_\beta^2 + C_{\alpha\beta}\hat{n}_\alpha\hat{n}_\beta, \quad (39)$$

where the six constant C's are functions of I, j, moments of inertia, and the strength of the single-particle potential V and deformation parameter γ through the definitions of the transformation coefficients in Eqs. (32). Their explicit forms are listed in Appendix B. Thus the particle-rotor Hamiltonian is approximately expressed in terms of two kinds of quantum numbers as

$$\begin{aligned} H_B &\simeq H_0 + \omega_\alpha + \omega_\beta + C_0 + (2\omega_\alpha + C_\alpha)\hat{n}_\alpha \\ &\quad + (2\omega_\beta + C_\beta)\hat{n}_\beta + C_{\alpha\alpha}\hat{n}_\alpha^2 + C_{\beta\beta}\hat{n}_\beta^2 + C_{\alpha\beta}\hat{n}_\alpha\hat{n}_\beta. \end{aligned} \quad (40)$$

The algebraic treatment is allowed within a stability region, whose boundary is defined by $[\omega^{(+)}\omega^{(-)}]^2 = [ab - (f+g)^2][ab - (f-g)^2] = 0$, giving

$$\begin{aligned} &[(A + |B|)(C + |D|) - (F - G)^2] \\ &\quad \times [(A - |B|)(C - |D|) - (F + G)^2] = 0. \end{aligned} \quad (41)$$

As shown in Fig. 1, this equation yields the boundary lines of instability in the $\gamma - I$ plane for various values of the scaling

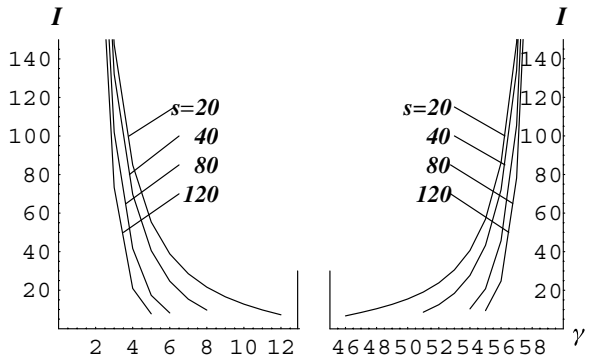

FIG. 1. The stability region of the algebraic solution in the $\gamma - I$ plane for the case of hydrodynamical moments of inertia. The boundary lines are shown only in the regions of $0^\circ < \gamma < 12^\circ$ and $46^\circ < \gamma < 60^\circ$. The stability region spreads in the upper side of each boundary line of instability, which is shown for four values of scaling parameter s (= 20, 40, 80, and 120).

factor s as a parameter. We observe in Fig. 1 that the boundary for the case of the hydrodynamical model ($0^\circ < \gamma < 60^\circ$) goes down with increasing s to allow a physical solution for a smaller I value. Narrow unstable regions occur only near $\gamma = 0^\circ$ and 60°, where the algebraic treatment breaks down. However, we do not consider the hydrodynamical model in such a region, in which one of three quantities $A_k = 1/\mathcal{J}_k$ diverges. For the case of the rigid-rotor model ($0^\circ < \gamma < 120^\circ$), the unstable regions near $\gamma = 0^\circ$ and 120° become much narrower. Since our interest is in the triaxially deformed nucleus, the existence of these unstable regions, which correspond to axially symmetric deformations, does not impede any practical application of the algebraic treatment in the subsequent section.

To clarify the physical meaning of two quantum numbers, n_α and n_β, which are the eigenvalues of $\hat{n}_\alpha$ and $\hat{n}_\beta$, we consider the pure rotor case, i.e., $V = 0$ in Eq. (1). Then formula (40) is reduced to a simple expression of the rotational energy

$$E_{\rm rot} \cong A_x R(R+1) - \frac{p+q}{2} n_\alpha^2 + \left(2R\sqrt{pq} + \sqrt{pq} - \frac{p+q}{2}\right)\left(n_\alpha + \frac{1}{2}\right), \quad (42)$$

where $p = A_y - A_x$, $q = A_z - A_x$, and $R = I - j + n_\beta$. Because in the symmetric limit $A_y = A_z$, formula (42) goes to the well-known expression

$$E_{\rm rot} = A_z R(R+1) - (A_z - A_x)(R - n_\alpha)^2. \quad (43)$$

The eigenvalue R can be regarded as an effective magnitude of the rotor angular momentum and $R - n_\alpha$ as its x component R_x. It turns out that these n_α and n_β are the same integers $n_{\alpha'}$ and $n_{\beta'}$ as defined in Eqs. (8) and (9). This allows us to interpret the quantum number n_α as the "precession" of $\vec{R}$ (the so-called "wobbling" [7]) because $R_x = R - n_\alpha$.

In this limit transformation (26) is reduced to

$$\hat{a} = \sqrt{\frac{I}{I-j}}(\eta_+\alpha + \eta_-\alpha^\dagger) - \sqrt{\frac{j}{I-j}}\beta^\dagger, \quad (44a)$$

$$\hat{b} = \sqrt{\frac{I}{I-j}}\beta - \sqrt{\frac{j}{I-j}}(\eta_+\alpha^\dagger + \eta_-\alpha), \quad (44b)$$

with

$$\eta_\pm = \left\{ \begin{matrix} 1 \\ \mathrm{sign}(p-q) \end{matrix} \right\} \left[\frac{1}{2}\left(\frac{p+q}{2\sqrt{pq}} \pm 1\right)\right]^{1/2}. \quad (44c)$$

We find that the relation $\hat{n}_\alpha - \hat{n}_\beta = \hat{n}_a - \hat{n}_b$ holds independently of I and j in the symmetric limit. On the other hand, α and β coincide with $\hat{a}$ and $\hat{b}$ in this limit where $\eta_+ = 1$ and $\eta_- = 0$, under the condition that the total spin I be much larger than j. Thus the quantum number n_β is interpreted as the "precession" of $\vec{j}$ about the intrinsic x axis because of Eqs. (10b). The precession of $\vec{R}$ and/or $\vec{j}$ gives rise to the precession of the total angular momentum $\vec{I}(= \vec{R} + \vec{j})$. Level formula (43) implies that all the states with common R and n_α degenerate in energy,

$$E^f_{\rm rot}(I, n_\alpha, n_\beta) = E^u_{\rm rot}(I-1, n_\alpha, n_\beta + 1) = E^f_{\rm rot}(I-2, n_\alpha, n_\beta + 2) = \cdots, \quad (45)$$

where the superscript $f(u)$ denotes a favored (unfavored) band. This degeneracy is lifted by the presence of the single-particle Hamiltonian $H_{\rm sp}$.

Because of the mixing of bosons $\hat{a}$ and $\hat{b}$, the physical contents of n_α and n_β change, but they keep the same values as in the symmetric limit whole through the adiabatic change of interaction parameter V and deformation parameters β_2 and γ. Thus the rotational bands can be classified in terms of a pair of quantum numbers (n_α, n_β) according to the restriction imposed by the D_2-selection rule in Eqs. (9).

IV. THE $E2$ AND $M1$ TRANSITION RATES

Exact diagonalization of H in Eq. (1) yields an eigensolution belonging to λth eigenvalue E^λ, which is expressed by the complete set of D_2-invariant wave functions with the coefficients of $C^{Ij\lambda}_{K\Omega}$ [14]:

$$\Psi(jIM\lambda) = \sum_{\Omega(\Omega>0)} \sum_{K(|K-\Omega|=\text{even})} C^{Ij\lambda}_{K\Omega} \sqrt{\frac{2I+1}{16\pi^2}} \times \left\{\mathcal{D}^I_{MK}(\theta_i)\phi^j_\Omega + (-1)^{I-j}\mathcal{D}^I_{M-K}(\theta_i)\phi^j_{-\Omega}\right\}, \quad (46)$$

where K and Ω are z components of $\vec{I}$ and $\vec{j}$. The $E2$ transition and $M1$ transition operators are given by

$$\mathcal{M}(E2,\mu) = \sqrt{\frac{5}{16\pi}} e\left[Q_0\mathcal{D}^2_{\mu 0} + Q_2\left(\mathcal{D}^2_{\mu 2} + \mathcal{D}^2_{\mu -2}\right)\right], \quad (47)$$

$$\mathcal{M}(M1,\mu) = \sqrt{\frac{3}{4\pi}}\mu_{\rm N} \sum_{\nu=0,\pm1} \left[(g_\ell - g_R)j_\nu + (g_s - g_\ell)s_\nu + g_R I_\nu\right]\mathcal{D}^1_{\mu\nu},$$

where $\mu_N = e\hbar/(2Mc)$, g_ℓ is the orbital g factor, g_s is the spin g factor, g_R is the effective g factor for the rotational motion, and Q_0 and Q_2 are components of the intrinsic quadrupole moment. The relation between the deformation parameter γ and the ratio of Q_2 to Q_0 is

$$\frac{Q_2}{Q_0} = -\frac{\tan\gamma}{\sqrt{2}}, \tag{48}$$

which is consistent with the definition of $\mathcal{J}^{\rm rig}$ and $H_{\rm sp}$ in Eqs. (3b) and (2b). We obtain the $B(E2)$ value from Eqs. (46) and (47) as

$$\begin{aligned} &B(E2; I_i\lambda_i \to I_f\lambda_f) \\ &= \frac{1}{2I_i+1}|\langle I_f\lambda_f||\mathcal{M}(E2)||I_i\lambda_i\rangle|^2 \\ &= \frac{5e^2}{16\pi}\Bigg|\sum_{\Omega(\Omega>0)}\sum_{K(|K-\Omega|=\text{even})}\Big[C^{I_f j\lambda_f *}_{K\Omega}Q_0\langle I_i K20|I_f K\rangle \\ &\quad + C^{I_f j\lambda_f *}_{K+2\Omega}Q_2\langle I_i K22|I_f K+2\rangle \\ &\quad + C^{I_f j\lambda_f *}_{K-2\Omega}Q_2\langle I_i K2-2|I_f K-2\rangle\Big]C^{I_i j\lambda_i}_{K\Omega}\Bigg|^2. \end{aligned} \tag{49}$$

Similarly, we obtain for the $M1$ transition

$$\begin{aligned} &B(M1; I_i\lambda_i \to I_f\lambda_f) \\ &= \frac{1}{2I_i+1}|\langle I_f\lambda_f||\mathcal{M}(M1)||I_i\lambda_i\rangle|^2 \\ &= \frac{3(\mu_N g_{\rm eff})^2}{4\pi}\Bigg|\sum_{\Omega(\Omega>0)}\sum_{K(|K-\Omega|=\text{even})}\Bigg[C^{I_f j\lambda_f *}_{K+1\Omega+1} \\ &\quad\times\sqrt{\frac{(j-\Omega)(j+\Omega+1)}{2}}\langle I_i K11|I_f K+1\rangle \\ &\quad - C^{I_f j-1\lambda_f *}_{K-1\Omega-1}\sqrt{\frac{(j+\Omega)(j-\Omega+1)}{2}}\langle I_i K1-1|I_f K-1\rangle \\ &\quad - C^{I_f j\lambda_f *}_{K\Omega}\Omega\langle I_i K10|I_f K\rangle + (-1)^{I_i-j}\delta_{\Omega,1/2}C^{I_f j\lambda_f *}_{1-K1-\Omega} \\ &\quad\times\frac{j+1/2}{\sqrt{2}}\langle I_i-K11|I_f 1-K\rangle\Bigg]C^{I_i j\lambda_i}_{K\Omega}\Bigg|^2 \end{aligned} \tag{50}$$

with $g_{\rm eff} = g_\ell - g_R + (g_s - g_\ell)/(2j)$.

Although the $B(E2)$ and $B(M1)$ values for the intraband and interband transitions can be calculated directly from the eigenfunctions of Hamiltonian (1) according to Eqs. (49) and (50), it is useful to calculate them by the algebraic method in order to find the selection rules for the transitions among the bands specified by different quantum numbers. For this purpose, we need the transformation coefficients between two boson Fock spaces, i.e., the one is generated on the quasi vacuum $|0\rangle_\alpha$ for quasibosons (α, β) and the other on the vacuum $|0\rangle_a$ for HP bosons $(\hat a, \hat b)$. Defining these overlaps is an extension of the coefficient G_{kl} [10,15,16] to the present case with two kinds of boson. We calculate such a set of the coefficients by applying the extended form of the generalized Wick theorem [17]:

$$\begin{aligned} &{}_a\langle 0|\hat a_1\hat a_2\ldots\hat a_m(\hat O)\alpha^\dagger_{m+1}\alpha^\dagger_{m+2}\ldots\alpha^\dagger_{2n}|0\rangle_\alpha \\ &= \sum\underbrace{BB\ldots B}_{\frac12(m-k)}\underbrace{CC\ldots C}_{k}\underbrace{AA\ldots A}_{n-\frac12(m+k)}. \end{aligned} \tag{51}$$

The summation extends over $(2n-1)!!$ terms corresponding to all the possible ways of contracting $2n$ boson operators, and the relevant factors are defined by

$$\begin{aligned} A_{\mu\nu} \equiv {}_a\langle 0|(\hat O)\alpha^\dagger_\mu\alpha^\dagger_\nu|0\rangle_\alpha, \quad B_{\mu\nu} \equiv {}_a\langle 0|\hat a_\mu\hat a_\nu(\hat O)|0\rangle_\alpha, \\ C_{\mu\nu} \equiv {}_a\langle 0|\hat a_\mu(\hat O)\alpha^\dagger_\nu|0\rangle_\alpha, \end{aligned} \tag{52}$$

with $(\hat O) \equiv 1/{}_a\langle 0|0\rangle_\alpha$. In Eqs. (51) and (52), the operator $\hat a_\mu$ represents either $\hat a_1 \equiv \hat a$ or $\hat a_2 \equiv \hat b$ and α_μ represents either $\alpha_1 \equiv \alpha$ or $\alpha_2 \equiv \beta$.

Our physical states, i.e., the eigenstates of H_B in relation (21), are expressed in terms of boson numbers n_α and n_β together with I and j:

$$|n_\alpha n_\beta, Ij\rangle = \frac{1}{\sqrt{n_\alpha! n_\beta!}}(\alpha^\dagger)^{n_\alpha}(\beta^\dagger)^{n_\beta}|0\rangle_\alpha. \tag{53}$$

Making use of the Wick theorem in Eq. (51) and the definitions of the matrix elements of $A_{\mu\nu}$, $B_{\mu\nu}$, and $C_{\mu\nu}$ in Eqs. (52), we calculate the overlap between $|n_a n_b, Ij\rangle$ and $|n_\alpha n_\beta, Ij\rangle$:

$$\begin{aligned} G^{Ij}_{n_a,n_b;n_\alpha,n_\beta} &\equiv \frac{{}_a\langle 0|\hat a^{n_a}\hat b^{n_b}(\alpha^\dagger)^{n_\alpha}(\beta^\dagger)^{n_\beta}|0\rangle_\alpha}{(n_a!n_b!n_\alpha!n_\beta!)^{1/2}} \\ &= \frac{{}_a\langle 0|0\rangle_\alpha}{(n_a!n_b!n_\alpha!n_\beta!)^{1/2}}{}_a\langle 0|\hat a^{n_a} \\ &\quad\times\hat b^{n_b}(\hat O)(\alpha^\dagger)^{n_\alpha}(\beta^\dagger)^{n_\beta}|0\rangle_\alpha. \end{aligned} \tag{54}$$

In this equation $n_a(= I-K)$ and $n_b(= j-\Omega)$ stand for the eigenvalues of $\hat n_a$ and $\hat n_b$, respectively. From now on K and Ω without a prime represent the x components of $\vec I$ and $\vec j$. Some simple examples of $G^{Ij}_{n_a,n_b;n_\alpha,n_\beta}$ are listed in Appendix C.

Associated with the change of quantization axis from the z to the x axis, the components of quadrupole moment must be transformed to

$$\begin{cases} Q_0 \\ Q_2 \end{cases} \to \begin{cases} Q_0' = -\frac12 Q_0 + \sqrt{\frac32}Q_2 \\ Q_2' = \frac12\left(\sqrt{\frac32}Q_0 + Q_2\right) \end{cases}. \tag{55}$$

Therefore, in the algebraic treatment Q_0 and Q_2 of Eq. (47) must be replaced with Q_0' and Q_2', respectively.

Making use of Eq. (5), we construct a manifestly D_2-invariant wave function in the laboratory frame as

$$\begin{aligned} &\langle IM|\mathcal{R}(\theta_i)\sqrt{2}\mathcal{P}\sum_\Omega^{\rm all}\sum_K^{\rm all}|IK\rangle|j\Omega\rangle\langle j\Omega|\langle IK|n_\alpha n_\beta, Ij\rangle \\ &= \sqrt{\frac{2I+1}{16\pi^2}}\sum_\Omega^{\rm all}\sum_{K(|K-\Omega|=\text{even})}\big[\mathcal{D}^I_{MK}(\theta_i)\phi^j_\Omega \\ &\quad + (-1)^{I-j}\mathcal{D}^I_{M-K}(\theta_i)\phi^j_{-\Omega}\big]G^{Ij}_{I-K,j-\Omega;n_\alpha,n_\beta}. \end{aligned} \tag{56}$$

A unit $\sum^{\rm all}_{\Omega,K}|IK\rangle|j\Omega\rangle\langle j\Omega|\langle IK| = 1$ is placed between $|n_\alpha n_\beta, Ij\rangle$ and $\sqrt{2}\mathcal{P}$ on the l.h.s. of Eq. (56) in order to convert

the basis vector $|n_\alpha n_\beta, Ij\rangle$ to the one in the angular-momentum representation. The operator $\mathcal{R}(\theta_i)$ rotates the principal axes in the body-fixed frame toward the laboratory frame. As proved in Sec. II C, H_B in relation (21) is D_2 invariant consistently within the second approximation and its eigenstates given by Eq. (53) belong to the $(r_1, r_2, r_3) = (+1, +1, +1)$ representation only if the quantum numbers n_α and n_β are restricted by the conditions in Eqs. (8) and (9). Our purpose of the projection introduced in Eq. (56) is not to construct the invariant state, but only to eliminate unnecessary components from the complete set $\{|IK\rangle|j\Omega\rangle\}$.

Although the summations of K and Ω extend also to negative values, we retain only a few terms whose K and Ω values do not much differ from I and j, respectively. Thus, within the framework of the algebraic treatment, the $B(E2)$ value is approximated as

$$\begin{aligned} &B\big(E2; I_i n_\alpha^i n_\beta^i \to I_f n_\alpha^f n_\beta^f\big) \\ &= \frac{5e^2}{16\pi}\Bigg|\sum_{\Omega(\Omega>0)}\sum_{K(K>0,|K-\Omega|=\text{even})}\Big[G^{I_f j}_{I_f-K, j-\Omega; n_\alpha^f, n_\beta^f} \\ &\quad\times Q_0'\langle I_i K 20|I_f K\rangle + G^{I_f j}_{I_f-K-2, j-\Omega; n_\alpha^f, n_\beta^f} \\ &\quad\times Q_2'\langle I_i K 22|I_f K+2\rangle + G^{I_f j}_{I_f-K+2, j-\Omega; n_\alpha^f, n_\beta^f} \\ &\quad\times Q_2'\langle I_i K 2-2|I_f K-2\rangle\Big]G^{I_i j}_{I_i-K, j-\Omega; n_\alpha^i, n_\beta^i}\Bigg|^2. \end{aligned} \tag{57}$$

In the same approximation, we obtain for the $M1$ transition from the initial state of $I_i = I$ to the final state of $I_f = I-1$,

$$\begin{aligned} &B\big(M1; I_i n_\alpha^i n_\beta^i \to I_f n_\alpha^f n_\beta^f\big) \\ &= \frac{3(\mu_N g_{\text{eff}})^2}{16\pi}\Bigg|\sum_{\Omega(\Omega>0)}\sum_{K(K>0,|K-\Omega|=\text{even})}\Big[G^{I_f j}_{I_f-K-1, j-\Omega-1; n_\alpha^f, n_\beta^f} \\ &\quad\times\sqrt{2(j-\Omega)(j+\Omega+1)}\langle I_i K 11|I_f K+1\rangle \\ &\quad- G^{I_f j}_{I_f-K+1, j-\Omega+1; n_\alpha^f, n_\beta^f}\sqrt{2(j+\Omega)(j-\Omega+1)} \\ &\quad\times\langle I_i K 1-1|I_f K-1\rangle - 2G^{I_f j}_{I_f-K, j-\Omega; n_\alpha^i, n_\beta^i} \\ &\quad\times\Omega\langle I_i K 10|I_f K\rangle\Big]G^{I_i j}_{I_i-K, j-\Omega; n_\alpha^i, n_\beta^i}\Bigg|^2. \end{aligned} \tag{58}$$

An approximation collecting only a few terms of $G^{Ij}_{n_a,n_b;n_\alpha,n_\beta}$ in the lowest-order products of $A_{\mu\nu}$, $B_{\mu\nu}$, and $C_{\mu\nu}$ is useful in deriving selection rules and to estimate the order of magnitude of the transition matrix elements, although it is not enough to reproduce the exact transition rates that are calculated from Eqs. (49) and (50). For simplicity, we employ an asymptotic estimation by assuming that I is large enough and that the difference of the I dependence of $G^{Ij}_{n_a,n_b;n_\alpha,n_\beta}$ between the initial and the final states is negligible. We drop the indices I and j from $G^{Ij}_{n_a,n_b;n_\alpha,n_\beta}$ and employ its abbreviation as $G_{n_a n_b n_\alpha n_\beta}$ for small n's. For example, if the yrast unfavored state with I $(I-j=\text{odd})$ has quantum numbers $(n_\alpha, n_\beta) = (1, 0)$, and the yrast favored state with $I-1$ has $(n_\alpha, n_\beta) = (0, 0)$, the ratios of interband $B(E2)$ and $B(M1)$ values to the intraband $B(E2)$ value in the lowest-order approximation are given by

$$\frac{B(E2; I10\to I-100)}{B(E2; I10\to I-210)} \sim \frac{6}{I}\tan^2\left(\gamma+\frac{\pi}{6}\right)\left(\frac{G_{0000}G_{1010}}{G_{0110}^2+G_{1010}^2}\right)^2, \tag{59a}$$

$$\frac{B(M1; I10\to I-100)}{B(E2; I10\to I-210)} \sim \frac{12}{5}\left(\frac{\mu_N g_{\text{eff}}}{eQ_2'}\right)^2\frac{j^2}{I}\left(\frac{G_{0000}G_{1010}}{G_{0110}^2+G_{1010}^2}\right)^2. \tag{59b}$$

In approximation (59a), we have used the relation among Q_0, Q_2, and γ in Eq. (48).

The ratios of interband $B(E2)$ and $B(M1)$ values to the intraband $B(E2)$ value from the state of I in the favored band with $(n_\alpha, n_\beta) = (0, 0)$ to the state of $I-1$ in the unfavored band with (1,0) are given by

$$\frac{B(E2; I00\to I-110)}{B(E2; I00\to I-200)} \sim \frac{2}{I}\left(\frac{G_{1010}}{G_{0000}}\right)^2, \tag{60a}$$

$$\frac{B(M1; I00\to I-110)}{B(E2; I00\to I-200)} \sim \frac{12}{5}\left(\frac{\mu_N g_{\text{eff}}}{eQ_2'}\right)^2 j\left(\frac{G_{0110}}{G_{0000}}\right)^2. \tag{60b}$$

Among the three overlaps, $G_{0000} = {}_a\langle 0|0\rangle_\alpha$, $G_{1010} = {}_a\langle 0|\hat{a}\alpha^\dagger|0\rangle_\alpha$, and $G_{0110} = {}_a\langle 0|\hat{b}\alpha^\dagger|0\rangle_\alpha$, $|G_{0110}|$ is much smaller than $|G_{0000}|$ and $|G_{1010}|$. The r.h.s. of Eq. (59a) is expected to be $3\tan^2(\gamma+\pi/6)(G_{0000}/G_{1010})^4$ times larger than the r.h.s. of relation (60a) if G_{0110}^2 is neglected in the denominator of relation (59a). Both ratios in relations (59a) and (60a) decrease as $1/I$ with increasing I. The transition rate with the factor G_{0110} is interpreted to be approximately "forbidden," and so the $M1$ transition from the favored state with I to the unfavored state with $I-1$ is forbidden. The r.h.s. of relation (60b) is expected to be $(I/j)(G_{0110}G_{1010}/G_{0000}^2)^2$ times smaller than the r.h.s. of relation (59b) if G_{0110}^2 is neglected in the denominator of relation (59b). When the scaling factor $s(=\mathcal{J}_0 V)$ is large, H_{sp} dominates irrespective of the value V. In this physical situation, $\vec{j}$ is well aligned to the x direction and $\hat{b}$ is not much mixed with $\hat{\alpha}$. Then the change in n_α costs less energy than does the change in n_β. In other words, $\vec{I}$ can precess with a lower cost in energy than $\vec{j}$ can. Then the $\hat{a}$ $(\hat{b})$ component dominates in $\hat{\alpha}$ $(\hat{\beta})$.

If the yrast unfavored state with I $(I-j=\text{odd})$ is specified by the quantum numbers $(n_\alpha, n_\beta) = (0, 1)$, and the yrast favored state with $I-1$ by $(0, 0)$, the ratios of interband $B(E2)$ and $B(M1)$ values to the intraband $B(E2)$ value in the lowest-order approximation are given by

$$\frac{B(E2; I01\to I-100)}{B(E2; I01\to I-201)} \sim \frac{6}{I}\tan^2\left(\gamma+\frac{\pi}{6}\right)\left(\frac{G_{0000}G_{1001}}{G_{0101}^2+G_{1001}^2}\right)^2, \tag{61a}$$

$$\frac{B(M1; I01\to I-100)}{B(E2; I01\to I-201)} \sim \frac{12}{5}\left(\frac{\mu_N g_{\text{eff}}}{eQ_2'}\right)^2\frac{j^2}{I}\left(\frac{G_{0000}G_{1001}}{G_{0101}^2+G_{1001}^2}\right)^2. \tag{61b}$$

The ratios of interband $B(E2)$ and $B(M1)$ values to the intraband $B(E2)$ value for the transitions from the state of I in the favored band with $(0, 0)$ to the state of $I-1$ in the unfavored band with $(0, 1)$ are given by

$$\frac{B(E2; I00 \to I-101)}{B(E2; I00 \to I-200)} \sim \frac{2}{I}\left(\frac{G_{1001}}{G_{0000}}\right)^2, \tag{62a}$$

$$\frac{B(M1; I00 \to I-101)}{B(E2; I00 \to I-200)} \sim \frac{12}{5}\left(\frac{\mu_N g_{\rm eff}}{eQ_2'}\right)^2 j\left(\frac{G_{0101}}{G_{0000}}\right)^2. \tag{62b}$$

In contrast to the cases of relations (59a) and (60a), both $B(E2)$ ratios in relations (61a) and (62a) include the factor $|G_{1001}|(=|_a\langle 0|\hat{a}\beta^\dagger|0\rangle_\alpha|)$, which is much smaller than $|G_{0000}|$ and $|G_{0101}|(=|_a\langle 0|\hat{b}\beta^\dagger|0\rangle_\alpha|)$. Therefore the $E2$ transitions between the unfavored state with (0,1) and the favored state with (0,0) are approximately forbidden, and their strengths are comparable in the order of magnitude. However, the lowest-order approximation is not enough, and higher-order contributions must be included to describe their proper staggering behavior.

The $B(M1)$ value for the transition from the favored state is approximately forbidden because of the factor G_{1001}^2. The r.h.s. of relation (61b) is expected to be $(j/I)(G_{1001}G_{0000}^2/G_{0101}^3)^2$ times smaller than the r.h.s. of relation (62b) if G_{1001}^2 is neglected in the denominator of relation (61b). In the case of a hydrodynamical model with small s, $H_{\rm rot}$ dominates and $\hat{a}$ and $\hat{b}$ are not much mixed, so that $|G_{1001}|$ becomes smaller than $|G_{0101}|$. In such a situation, the $B(M1)$ ratio from the unfavored band becomes smaller than that from the favored band. From relations (59)–(62), the $B(M1)$ ratio from the unfavored state decreases with I, while the ratio from the favored state remains in a stable value almost independent of I.

V. NUMERICAL ANALYSIS

A. Comparison with the exact results in energy levels

We performed a numerical analysis by putting $j = 13/2$ and compared the algebraic energy levels [formula (40)] determined by (n_α, n_β) with the exact results obtained from original Hamiltonian (1) as functions of γ. We adopt $\mathcal{J}^{\rm hyd}$ in Eq. (3a) and show the case of $s = 20$ in Fig. 2 and $s = 80$ in Fig. 3. In both cases, $\mathcal{J}_0$ is chosen to be 50 MeV^{-1}, and the comparison is made for four low-lying energy levels of $I = 45/2$ belonging to the favored bands ($I - j =$ even) in the left-hand panels (a), while in the right-hand panels (b), we show the case of four low-lying energy levels of $I = 43/2$ belonging to the unfavored bands ($I - j =$ odd). We find excellent agreement of the algebraic results with the exact ones in a wide range of γ except for the regions of $\gamma \leqslant 15^\circ$ and $\gamma \geqslant 45^\circ$. In the hydrodynamical model our prescription cannot be extended to the axially symmetric limits at $\gamma = 0^\circ$ and $\gamma = 60^\circ$, where either $A_z = 1/\mathcal{J}_z^{\rm hyd}$ or $A_y = 1/\mathcal{J}_y^{\rm hyd}$ diverges.

The physical content of each level can be understood from the assigned quantum numbers. In Fig. 2(a), the yrast favored band is specified by $(n_\alpha, n_\beta) = (0, 0)$, which implies that $R = R_x = I - j(=16)$, and both $\vec{I}$ and $\vec{j}$ are stretched along the x axis. The second band is specified by $(0, 2)$, in which $\vec{j}$ precesses around the x axis and $\vec{R}$ is stretched as $R = R_x$ $(= 18)$. The band specified by $(1, 1)$ appears as the third, and the one by $(2, 0)$ as the fourth. The third band given by $(1, 1)$ corresponds to $R = I - j + 1(= 17)$ and $R_x = R - 1(= 16)$, where both $\vec{j}$ and $\vec{R}$ precess. The fourth band given by $(2, 0)$ corresponds to $R = I - j(= 16)$ and $R_x = R - 2(= 14)$. In this state $\vec{j}$ is stretched, while $\vec{R}$ precesses around the x axis. In Fig. 2(b), I is smaller than that in Fig. 2(a) by one unit. The unfavored yrast band in Fig. 2 has (0,1), where $R = R_x = I - j + 1(= 16)$, and $\vec{j}$ precesses and $\vec{R}$ is stretched. The second band with (1,0) has $R = I - j(= 15)$ and $R_x = R - 1(= 14)$, and $\vec{j}$ is stretched and $\vec{R}$ precesses. The third band with (0,3) has $R = R_x = I - j + 3(= 18)$, and $\vec{j}$ precesses and $\vec{R}$ is stretched. The fourth band with (1,2) has $R = I - j + 2(= 17)$ and $R_x = R - 1(= 16)$, and both $\vec{j}$ and $\vec{R}$ precess.

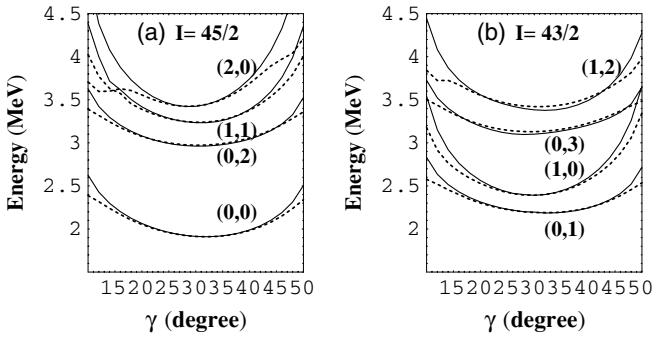

FIG. 2. The energy levels in units of MeV calculated with the hydrodynamical moments of inertia for the case of $s = 20$ as functions of the deformation parameter γ in units of degrees. The solid curves indicate the algebraic solutions with (n_α, n_β), and the dotted curves the exact results. (a) $I = 45/2$, (b) $I = 43/2$.

In contrast to Fig. 2 ($s = 20$), we observe in Fig. 3 ($s = 80$) that the second favored band is specified by (2,0), and the yrast unfavored band by (1,0), which implies that these bands are characterized by the precession of $\vec{I}$ rather than that of $\vec{j}$. This crossover, in which quantum numbers of the yrast unfavored band change from (0,1) to (1,0), takes place at $s \sim 50$. It is remarkable that the $(0, 1)$ state with the precession of $\vec{j}$ comes down as the unfavored yrast state in the case of $s = 20$, while

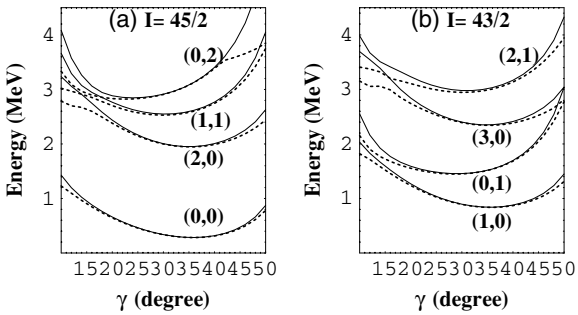

FIG. 3. The energy levels in units of MeV calculated with the hydrodynamical moments of inertia for the case of $s = 80$ as functions of the deformation parameter γ in units of degrees. The meanings of the curves are as defined in Fig. 2.

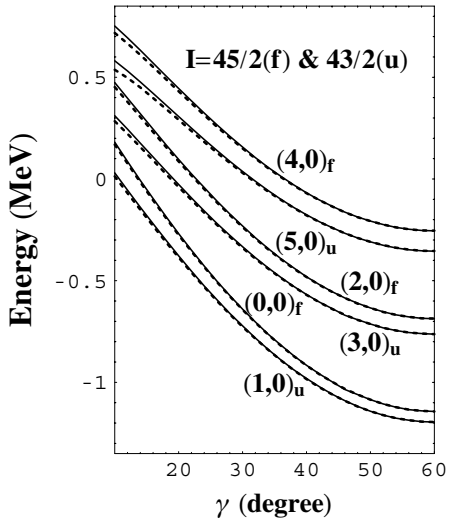

FIG. 4. The energy levels in units of MeV calculated with the rigid-body moments of inertia for the case of $s = 120$ as functions of γ in units of degrees. The solid curves represent the algebraic solutions for $I = 45/2$ [the favored band with $(n_\alpha, n_\beta)_f$] and for $I = 43/2$ [the unfavored band with $(n_\alpha, n_\beta)_u$]. The dotted curves represent the exact results.

the (1, 0) state with the precession of $\vec{R}$ comes down in the case of $s = 80$. This difference is clearly understood from Eq. (43). The excitation of the (0,1) state costs less energy than that of the (1,0) state, so long as $2\mathcal{J}_z < \mathcal{J}_x$ at large $I - j$. This condition is fully satisfied in the small s, but not in the large s.

For the case of the rigid-body moments of inertia, it is confirmed that two low-lying levels for both favored and unfavored bands keep the same quantum numbers, at least in a range of $18 \leqslant s \leqslant 180$, and no crossover occurs between the bands with different characteristics, which is seen for the case of hydrodynamical moments of inertia. In Fig. 4 we show the behavior of energy levels for the case of $s = 120$ with $\mathcal{J}_0 = 62\ \mathrm{MeV}^{-1}$ and $\beta_2 = 0.38$ in Eq. (3b). The algebraic solutions (solid curves) are compared with the exact results (dotted curves) calculated from original Hamiltonian (1) as functions of γ for three low-lying energy levels of $I = 45/2$ (the favored bands denoted by the subscript and for three low-lying energy levels of $I = 43/2$ (the unfavored bands denoted by the subscript u). We find that the algebraic energy levels reproduce the exact results much better for the rigid-body model than for the hydrodynamical model. The algebraic formula becomes exact at $\gamma = 60^\circ$, where $\mathcal{J}_y^{\mathrm{rig}} = \mathcal{J}_z^{\mathrm{rig}}$, and gradually deviates with increasing or decreasing γ. However, such a deviation is slight, because the change of the rigid-body moments of inertia is slow and the differences among three moments of inertia are much smaller than those of the hydrodynamical model. Moreover, $1/\mathcal{J}^{\mathrm{rig}}$ does not diverge at $\gamma = 0^\circ$, which allows a better fit at small γ. The algebraic formula with $\mathcal{J}^{\mathrm{rig}}$ predicts the behavior of low-lying levels with sufficient accuracy to assign the quantum numbers to each level without ambiguity.

To investigate how the inclusion of the particle-rotor coupling together with the single-particle potential affects the energy level of the simple pure rotor model and how the second approximation improves the first approximation, we refer to the energy difference between the unfavored yrast level $E(I, n_\alpha = 1, n_\beta = 0)$ and the favored yrast level $E(I, n_\alpha = 0, n_\beta = 0)$ in what follows. We define

$$\Delta E_a = E(I, 1, 0) - \tfrac{1}{2}[E(I-1, 0, 0) + E(I+1, 0, 0)] \quad (63)$$

and a similar quantity in an alternative form

$$\Delta E_b = \tfrac{1}{2}[E(I-1, 1, 0) + E(I+1, 1, 0)] - E(I, 0, 0), \quad (64)$$

which measure the one-phonon energy in the wobbling model [7], where the one-phonon energy for an even nucleus is given by

$$\Delta E_{\mathrm{BM}} = 2I\sqrt{(A_y - A_x)(A_z - A_x)}. \quad (65)$$

Numerical calculations are performed for the case of rigid-body moments of inertia with the set of parameters $s = 120$, $\mathcal{J}_0 = 52.4\ \mathrm{MeV}^{-1}$ and $\gamma = 17^\circ$, as adopted in Sec. V C.

In Fig. 5(a), we compare the energy difference ΔE_a calculated in three ways, i.e., the first approximation and the second approximation that are defined in Sec. II C and the exact diagonalization together with the wobbling model ΔE_{BM}. In Fig. 5(b), a similar comparison is also made for the energy difference ΔE_b calculated in three ways together with ΔE_{BM}. The second approximation is denoted by "2nd" in the figure, the first approximation by "1st", and the wobbling model by "BM". Note that, in "1st", corresponding quantities are given by eliminating $A_{yzx} + a_{yzx}$ in H_0 in Eq. (22),

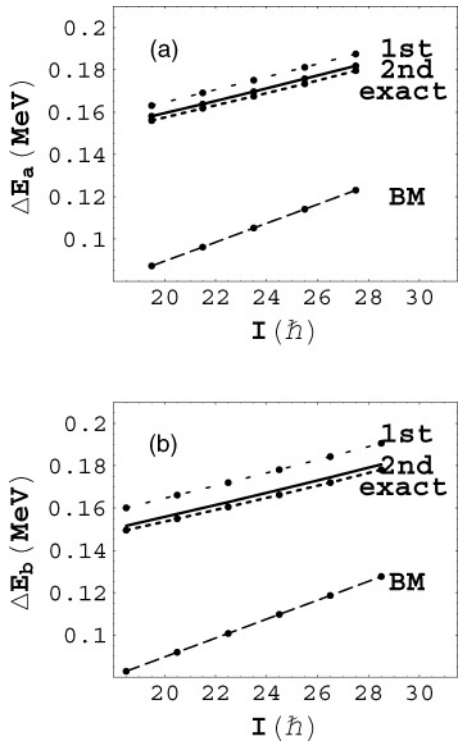

FIG. 5. A comparison of four kinds of theoretical energy differences between the unfavored yrast level and the favored yrast level as functions of angular momentum I. The energy differences are calculated by two kinds of approximation, the exact diagonalization and the wobbling model. (a) energy difference ΔE_a, (b) ΔE_b. The definitions of ΔE are given by Eqs. (63)–(65) in the text.

and 1/2 and 1/4 in the parentheses of A, B, C, and D in Eqs. (25). We apply the algebraic treatment to the Hamiltonian with newly defined H_0, A, B, C, and D without H_4 in Eq. (24). We observe that "2nd" improves "1st", especially for ΔE_b, and simulates quite well "exact". Note that "1st" in the present calculation includes both particle-rotor coupling and single-particle potential. There are large discrepancies between the results of "BM" and the others, and the gradient of "BM" is larger than that of the others. This discrepancy is partly compensated for by the particle-rotor coupling, as discussed in Ref. [9].

B. Comparison with the exact results in the transition rates

At first, a comparison is made for the absolute values of $B(E2)$ and $B(M1)$ between the exact results and the approximate results. The exact results are based on the formulas in Eqs. (49) and (50) and the approximate results on the formulas in Eqs. (57) and (58). In Table I we show the numerical results for the initial state of $I = 43/2$ (unfavored band) and 45/2 (favored band) in the rigid-body moments of inertia with $s = 120$, $\gamma = 17^\circ$, $Q_0 = 10$ b, and $g_{\rm eff} = 0.394$. Note that the wave functions depend on only the scaling parameter s. In the first column of Table I, $B(E2)_{\rm out}$ and $B(M1)_{\rm out}$ denote the interband (out-of-band) transitions from I to $I-1$, and $B(E2)_{\rm in}$ the intraband (in-band) transition from I to $I-2$. In the first row of Table I, "$\Delta n = 0$" stands for the approximation taking only terms with $G^{Ij}_{n_a,n_b;n_\alpha,n_\beta}$ whose subscripts satisfy $n_a + n_b - n_\alpha - n_\beta = 0$ ($n_\alpha + n_\beta = 0$, or 1), and "$\Delta n = 2$" for the approximation taking $n_a + n_b - n_\alpha - n_\beta = 2$ in addition to the "$\Delta n = 0$." In Table I we see that the overall values in the $\Delta n = 0$ approximation are not so bad, although the convergence of each value to the exact one is not enough, especially for the $B(M1)_{\rm out}$ value. Thus we may conclude that we can infer the selection rule and estimate the order of magnitude for the transition rates from the $\Delta n = 0$ approximation. It is remarked that the exact values are comparable with the experimental data for ^{163}Lu [4]. For example, our theoretical value at $I = 45/2$, $B(E2)_{\rm in} = 2.393$ (see the ninth row in Table I), is comparable with the experimental value $B(E2)_{\rm in} = 3.07^{+0.48}_{-0.43}$. With the same set of parameters our theoretical values at $I = 47/2$, $B(E2)_{\rm in} = 2.372$, $B(E2)_{\rm out} = 0.530$, and $B(M1)_{\rm out} = 0.028$, are comparable with the experimental values $B(E2)_{\rm in} = 2.56^{+0.57}_{-0.44}$, $B(E2)_{\rm out} = 0.54^{+0.13}_{-0.11}$, and $B(M1)_{\rm out} = 0.017^{+0.006}_{-0.005}$, respectively.

TABLE I. A comparison of $B(E2)$ and $B(M1)$ between exact results and approximate results.

$I = 43/2$	Exact	$\Delta n = 0$	$\Delta n = 2$
$B(E2)_{\rm out}$	0.577	0.547	0.431
$B(E2)_{\rm in}$	2.346	1.478	1.663
$B(E2)_{\rm out}/B(E2)_{\rm in}$	0.246	0.370	0.259
$B(M1)_{\rm out}$	0.033	0.054	0.089
$B(M1)_{\rm out}/B(E2)_{\rm in}$	0.014	0.036	0.054
$I = 45/2$	Exact	$\Delta n = 0$	$\Delta n = 2$
$B(E2)_{\rm out}$	0.069	0.159	0.058
$B(E2)_{\rm in}$	2.393	1.954	2.029
$B(E2)_{\rm out}/B(E2)_{\rm in}$	0.029	0.081	0.028
$B(M1)_{\rm out}$	0.15×10^{-3}	0.10×10^{-3}	0.38×10^{-2}
$B(M1)_{\rm out}/B(E2)_{\rm in}$	0.61×10^{-4}	0.53×10^{-4}	0.19×10^{-2}

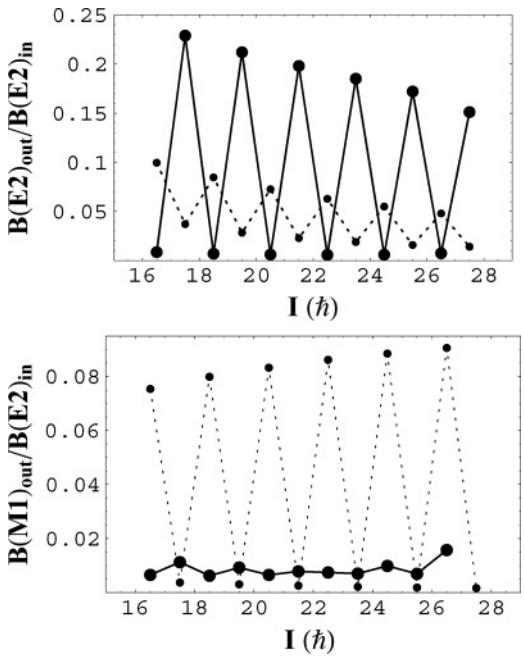

FIG. 6. A comparison of $B(E2)_{\rm out}/B(E2)_{\rm in}$ (upper panel) and $B(M1)_{\rm out}/B(E2)_{\rm in}$ (lower panel) between the cases of $s = 20$ and 80 with the hydrodynamical moments of inertia at $\gamma = 17^\circ$. The small circles connected with dotted lines denote the case of $s = 20$, and the large circles connected with solid lines denote the case of $s = 80$.

In Fig. 6, we compare the ratios of $B(E2)_{\rm out}/B(E2)_{\rm in}$ and $B(M1)_{\rm out}/B(E2)_{\rm in}$ between two cases of $s = 20$ and 80 with the hydrodynamical moments of inertia at $\gamma = 17^\circ$. The results are based on the exact diagonalization of the total Hamiltonian. The large circles connected by the solid lines represent $s = 80$, and the small circles connected by the dotted lines represent $s = 20$. It is clearly seen that both results give the staggering behavior between the transitions from the unfavored band and the transitions from the favored band, which have already been discussed with respect to relations (59)–(62). The staggering is just out of phase between the cases of $s = 20$ and $s = 80$. This out-of-phase property is due to the difference in the quantum numbers, i.e., the quantum numbers (1,0) in $s = 80$ and (0,1) in $s = 20$.

In the case of $s = 80$, both transition rates from the unfavored band are larger than those from the favored band, as is seen in relations (59) and (60). However, the amplitude of the staggering in $B(M1)_{\rm out}/B(E2)_{\rm in}$ is not so large because of a small kinematical factor j/I in the "allowed" transition rate. These expectations are demonstrated by the large circles connected by the solid lines in Fig. 6. These results support the interpretation that the unfavored band has the character of the precession of I rather than that of j.

In the case of $s = 20$, the $E2$ transitions from both the unfavored state and the favored state are approximately forbidden because of the factor of G^2_{1001}, so that relatively

small amplitude of the staggering is expected, which is shown in the upper panel of Fig. 6. To reproduce the correct behavior of the staggering, we must take a further step in the approximation by taking up to $n_a + n_b - n_\alpha - n_\beta = 4$. The $\Delta I = 1$ $E2$ transition between the unfavored band with (0,1) and the favored band with (0,0) is suppressed because of the orthogonality of the relevant single-particle states. We confirmed also at $\gamma = 20^\circ$ for $I = 45/2$ that the ratio of $B(E2)_{\rm out}/B(E2)_{\rm in}$ is 0.016 for $s = 20$, while it is 0.276 for $s = 80$. As for $B(M1)_{\rm out}/B(E2)_{\rm in}$, the ratio from the unfavored state is approximately forbidden because of the factor G^2_{1001}, while the ratio from the favored state is allowed. Thus the large amplitude of the staggering is expected, which is demonstrated by the small circles connected by the dotted lines in the lower panel of Fig. 6. Thus the lowest-order estimations in relations (59)–(62) provide the selection rules and enable us to predict basic properties of the transitions.

In Fig. 7, we show the γ dependence of $B(E2)$ and $B(M1)$ transitions at $I = 43/2$ (favored band) for $s = 80$ in the case of rigid-body moments of inertia. We choose $Q_0 = 9\,$b and $g_{\rm eff} = 0.394$. In the upper panel, $B(E2)_{\rm out}$ is denoted by the small filled circles connected by the dotted lines and $B(E2)_{\rm in}$ by the large filled circles connected by the solid line as functions of γ. In the lower panel, $B(M1)_{\rm out}$ is denoted by the small filled circles connected by the dotted curve as a function of γ. The results are based on the exact diagonalization of the total Hamiltonian. $B(E2)_{\rm in}$ decreases with increasing γ, while $B(E2)_{\rm out}$ increases. The γ dependence of $B(M1)_{\rm out}$ increases slowly with γ and remains almost constant.

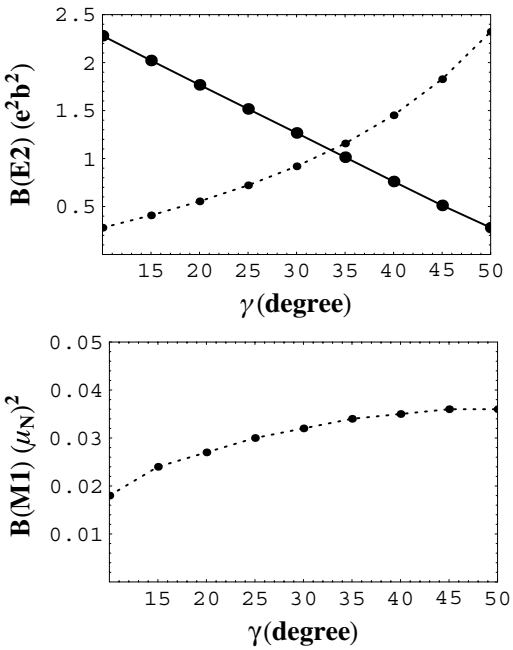

FIG. 7. The γ dependence of $B(E2)$ and $B(M1)$ at $I = 43/2$ for $s = 80$ in the rigid-body moments of inertia. The upper panel is for $B(E2)_{\rm out}$ (small closed circles connected by the dotted curve) and $B(E2)_{\rm in}$ (large closed circles connected by the solid line) as functions of γ in unit of e^2b^2. The lower panel is for $B(M1)_{\rm out}$ (small closed circles connected by the dotted curve) as a function of γ in unit of μ_N^2.

This behavior is also understood from the approximate solutions. If we take only the lowest-order $G^{Ij}_{n_a,n_b;n_\alpha,n_\beta}$ as in relations (59) and assume that G_{1010} and G_{0000} do not differ much from 1 asymptotically at large I, then $B(E2)_{\rm in}$, $B(E2)_{\rm out}$, and $B(M1)_{\rm out}$ become

$$B(E2)_{\rm in} \propto (Q_2')^2 = \frac{Q_0^2}{8}(\sqrt{3} - \tan\gamma)^2,$$
$$B(E2)_{\rm out} \propto (Q_0')^2\frac{3}{I} = \frac{3Q_0^2}{4I}(\sqrt{3}\tan\gamma + 1)^2, \qquad (66)$$
$$B(M1)_{\rm out} \propto (\mu_N g_{\rm eff})^2\frac{j^2}{I}.$$

From these expressions it is easily understood that $B(E2)_{\rm in}$ decreases and $B(E2)_{\rm out}$ increases with increasing $\tan\gamma$. The $B(M1)_{\rm out}$ value does not depend on γ explicitly, and so it does not show any drastic γ dependence.

C. Comparison with the experimental data

Four TSD bands are observed experimentally in ^{163}Lu [1–3], i.e., TSD1 and TSD3 bands as the favored bands and TSD2 and probably TSD4 bands as the unfavored bands. In the hydrodynamical model, if s is small (<50), the TSD1 band is characterized by the quantum numbers (0,0), the TSD2 band by (0,1), the TSD3 band by (0,2), and the TSD4 by (1,0). On the other hand, if s is large (>50), the TSD2 band is specified by (1,0), the TSD3 band by (2,0), and the TSD4 by (3,0).

In the rigid-rotor model, the TSD1 band is characterized by the quantum numbers (0,0), the TSD2 band by (1,0), the TSD3 band by (2,0), and the TSD4 band by (3,0). We have confirmed that these quantum numbers do not change in the region of $18.4 \leqslant s \leqslant 120$. Although there is no difference in quantum numbers for TSD1, TSD2, and TSD3 between the rigid-body model and the hydrodynamical model with $s = 80$, the TSD2, level of I is always higher in energy than the TSD1 level of $I + 1$ for the hydrodynamical model, while their ordering is reversed for the rigid-body model.

In the upper panel of Fig. 8, we compare $B(E2)_{\rm out}/B(E2)_{\rm in}$ at $\gamma = 17^\circ$ with the experimental values [1] as functions of I in units of $\hbar$. In the lower panel of Fig. 8, we compare $B(M1)_{\rm out}/B(E2)_{\rm in}$ in units of $\mu_N^2/({\rm eb})^2$ at $\gamma = 17^\circ$ with the experimental values as functions of I. The theoretical values in both panels are obtained from the exact diagonalization of the total Hamiltonian. In the lower panel, the theoretical value is normalized at $I = 51/2$, as $B(M1)_{\rm out}/B(E2)_{\rm in}$ values depend on the ratio of $g_{\rm eff}/Q_0$, while $B(E2)_{\rm out}/B(E2)_{\rm in}$ does not depend on the input parameter Q_0.

In Figs. 9, 10, and 11, the algebraic energy levels of Lu isotopes are compared with the experimental level schemes [1, 2,5,6]. We adopt $s = 120$ with $\mathcal{J}_0 = 52.4\,{\rm MeV}^{-1}$ and $\beta_2 = 0.38$ for all the Lu isotopes, and the bandhead energy of the TSD1 band is shifted to the experimental energy in each isotope. It is remarkable that the overall trend of the level schemes of the TSD bands in ^{163,165,167}Lu together with the electromagnetic transition rates are consistently well reproduced by the rigid-body model. In particular, the relative level orderings between different TSD bands are correctly reproduced in each isotope. However, some algebraic levels near the bandheads are located

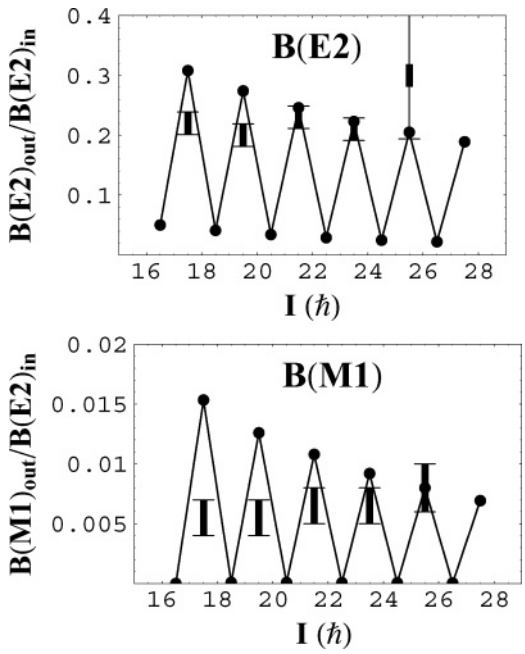

FIG. 8. A comparison between the theoretical and experimental ratios of $B(E2)_{\rm out}/B(E2)_{\rm in}$ (upper panel) and $B(M1)_{\rm out}/B(E2)_{\rm in}$ in units of $\mu_{\rm N}^2/({\rm eb})^2$ (lower panel) as functions of I in units of $\hbar$. The theoretical results with the rigid-body moments of inertia for the case of $s = 120$ and $\gamma = 17^\circ$ are represented by filled circles. The experimental data are from Ref. [1].

lower than the experimental ones. The rigid-body model is preferable, especially for reproducing the experimental level spectra. To obtain a better fit to the experimental level scheme, we need some optimization of the parameter set.

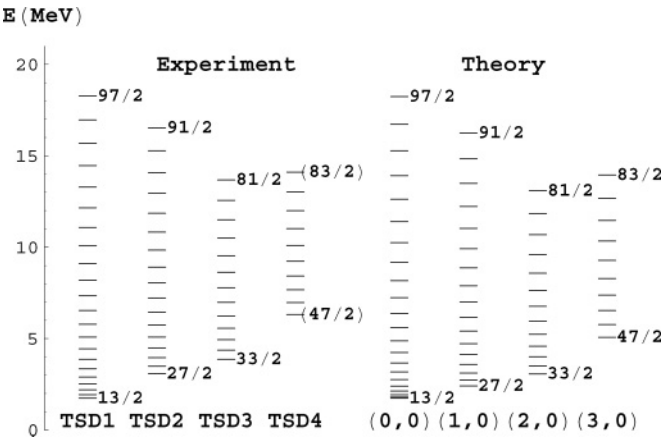

FIG. 9. A comparison between the experimental and the algebraic energy levels for ^{163}Lu in unit of MeV calculated with the rigid-body moments of inertia of $\gamma = 17^\circ$ for $s = 120$. A pair of numerals in the parentheses below the theoretical level scheme of each rotational band stands for the assigned quantum numbers (n_α, n_β). The half-integers assigned to the highest and the lowest levels in each band denote the angular momentum identified experimentally, while those in the bracket are not yet identified. The experimental data are from Refs. [1–3].

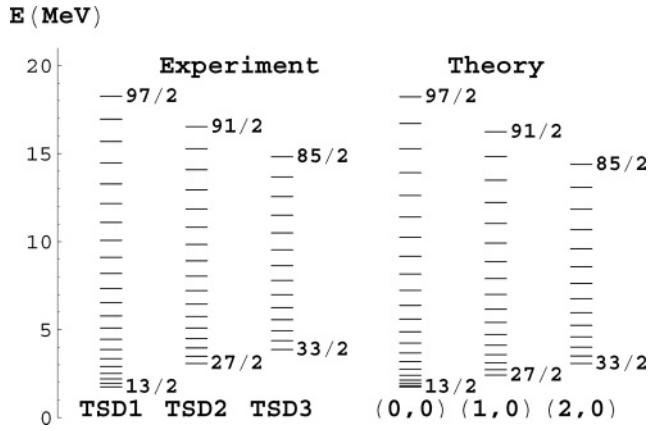

FIG. 10. A comparison between the experimental and the algebraic energy levels for ^{165}Lu in units of MeV calculated with the rigid-body moments of inertia of $\gamma = 17^\circ$ for $s = 120$. The experimental data are from Ref. [5]. For further details, see Fig. 9.

The pairing interaction is not included in the present model. The pairing correlation and the effect of shell filling may play some roles in the levels near the bandheads, especially for the isotopes ^{165,163}Lu. In such a case a theoretical treatment based on the quasiparticle picture is needed to describe the interaction of many particles distributed in relevant single-particle orbitals [9].

We investigate in detail the behavior of level distances in the case of ^{163}Lu. In Fig. 12, we compare the algebraic and the experimental level distances of the unfavored (TSD2) and the favored (TSD3) levels from the favored yrast level (TSD1) as defined by

$$\begin{aligned}\Delta E({\rm TSD2}-1) &= E({\rm TSD2}, I) - \tfrac{1}{2}[E({\rm TSD1}, I-1) \\ &\quad + E({\rm TSD1}, I+1)], \\ \Delta E({\rm TSD3}-1) &= E({\rm TSD3}, I) - E({\rm TSD1}, I).\end{aligned} \tag{67}$$

As seen in Fig. 12, theoretical results simulate the experimental values only in a region of $61/2 < I < 81/2$, but the decrease

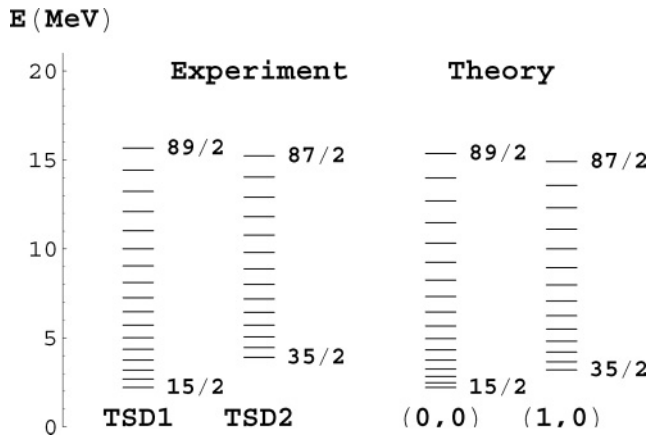

FIG. 11. A comparison between the experimental and the algebraic energy levels for ^{167}Lu in units of MeV calculated with the rigid-body moments of inertia of $\gamma = 17^\circ$ for $s = 120$. The experimental data are from Ref. [6]. For further details, see Fig. 9.

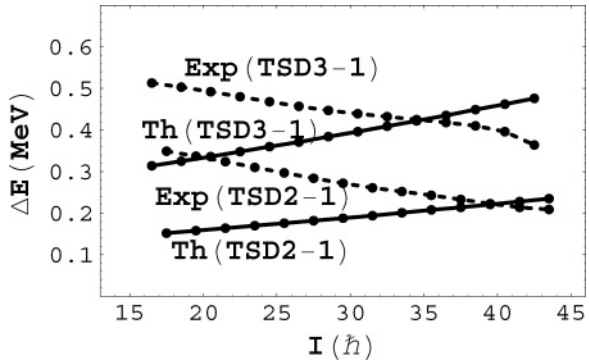

FIG. 12. A comparison of theoretical energy differences with experimental ones as functions of angular momentum I. The energy difference between TSD2 and TSD1 bands is indicated by "(TSD2–1)", and between TSD3 and TSD1 bands by "(TSD3–1)". The solid lines stand for the algebraic solutions, as indicated by "Th", while the dotted lines indicate the experimental data by "Exp". Experimental energy levels are take from Refs. [1–3], and the energy of the $I = 85/2$ level in the TSD3 band is from Ref. [18]. The definitions of energy difference ΔE are given by Eqs. (67) in the text.

of the level distances with increasing I cannot be reproduced by the particle-rotor model with constant moments of inertia.

VI. CONCLUSION

We have developed an algebraic method by applying the HP boson expansion method to the particle-rotor model. It is important to include the next-to-leading-order terms in order to maintain the D_2 invariance of the Hamiltonian, as well as to reproduce rotational energy spectra. Two quantum numbers (n_α, n_β) come out from two kinds of bosons representing commuting angular momenta, i.e., the total angular momentum $\vec{I}$ and the angular momentum of a valence nucleon $\vec{j}$. The quantum numbers are assigned uniquely to each rotational band by comparison of the algebraic energy formula with the exact energy obtained from the diagonalization of the total Hamiltonian. The agreement of both energies is surprisingly accurate, especially for the rigid-body model.

Two quantum numbers represent the precessions of $\vec{I}$ and $\vec{j}$ as a consequence of the Coriolis interaction. In the pure rotor case ($V = 0$), the magnitude of the rotor angular momentum R and its x component R_x are expressed in terms of two quantum numbers as $R = I - j + n_\beta$ and $R_x = R - n_\alpha$, and consequently n_α may be regarded as representing the precession of the rotor, i.e., the wobbling.

The algebraic method is extended to derive the selection rules in the electromagnetic transitions referring to the quantum numbers. Starting from the eigenstates in the quasiboson space $\{|n_\alpha n_\beta; Ij\rangle\}$, we prepare the explicit forms of the D_2-invariant wave functions of rotational states and express the transition matrix elements in terms of the overlap of $\langle n_a n_b; Ij|n_\alpha n_\beta; Ij\rangle$. The selection rules are inferred from the lowest-order overlaps.

As realistic examples, the algebraic method is applied to the odd-A isotopes ^{163,165,167}Lu. The particle-rotor Hamiltonian with the rigid-body moments of inertia and with only one set of parameters reproduces overall trends of the energy spectra along the TSD rotational bands in three odd-A nuclei, i.e., TSD1, TSD2, TSD3, and TSD4 in ^{163}Lu; TSD1, TSD2, and TSD3 in ^{165}Lu; and TSD1 and TSD2 in ^{167}Lu. From the calculations with the rigid-body moments of inertia, we find that preferable assignments of quantum numbers are $(n_\alpha, n_\beta) = (0, 0)$ for TSD1 in ^{163,165,167}Lu, $(1, 0)$ for TSD2 in ^{163,165,167}Lu, $(2, 0)$ for TSD3 in ^{163,165}Lu, and $(3, 0)$ for TSD4 in ^{163}Lu.

We have shown that the exact calculation with the rigid-rotor model reproduces the $B(E2)$ and $B(M1)$ values measured for ^{163}Lu in a recent experiment [4] as well as the ratios of $B(E2)_{\rm out}/B(E2)_{\rm in}$ and $B(M1)_{\rm out}/B(E2)_{\rm in}$. Owing to quantum numbers, the characteristic properties of the electromagnetic transition rates are well interpreted in terms of the selection rules from the approximate algebraic formula. Since the present algebraic method treats two angular momenta $\vec{I}$ and $\vec{j}$ evenly, it will be widely applicable to the other system that is composed of two interacting angular momenta.

ACKNOWLEDGMENT

The authors express their sincere thanks to W. Bentz for his careful reading of the manuscript.

APPENDIX A: PARAMETRIZATION OF BOSON TRANSFORMATION

The most general boson Bogoliubov transformation connecting original HP boson operators $(\hat{a}, \hat{b}, \hat{a}^\dagger, \hat{b}^\dagger)$ to new quasiboson operators $(\alpha, \beta, \alpha^\dagger, \beta^\dagger)$ is parametrized as

$$\begin{pmatrix} \hat{a} \\ \hat{b} \\ \hat{a}^\dagger \\ \hat{b}^\dagger \end{pmatrix} = \begin{bmatrix} \cos\chi & \sin\chi & 0 & 0 \\ -\sin\chi & \cos\chi & 0 & 0 \\ 0 & 0 & \cos\chi & \sin\chi \\ 0 & 0 & -\sin\chi & \cos\chi \end{bmatrix} \times \begin{bmatrix} \cosh\vartheta & 0 & \sinh\vartheta & 0 \\ 0 & \cosh\varphi & 0 & \sinh\varphi \\ \sinh\vartheta & 0 & \cosh\vartheta & 0 \\ 0 & \sinh\varphi & 0 & \cosh\varphi \end{bmatrix} \times \begin{bmatrix} \cos\psi & \sin\psi & 0 & 0 \\ -\sin\psi & \cos\psi & 0 & 0 \\ 0 & 0 & \cos\psi & \sin\psi \\ 0 & 0 & -\sin\psi & \cos\psi \end{bmatrix} \begin{pmatrix} \alpha \\ \beta \\ \alpha^\dagger \\ \beta^\dagger \end{pmatrix}. \tag{A1}$$

This factorization of the transformation is an extension of the Bloch-Messiah theorem [13] to the boson case. Therefore, eight transformation coefficients introduced in Eq. (26) in the text can be parametrized by

$$\begin{aligned} u_+ &= \cos\chi\cos\psi\cosh\vartheta - \sin\chi\sin\psi\cosh\varphi, \\ v_+ &= -\sin\chi\cos\psi\cosh\vartheta - \cos\chi\sin\psi\cosh\varphi, \\ u_- &= \cos\chi\cos\psi\sinh\vartheta - \sin\chi\sin\psi\sinh\varphi, \\ v_- &= -\sin\chi\cos\psi\sinh\vartheta - \cos\chi\sin\psi\sinh\varphi, \end{aligned} \tag{A2}$$

and

$$\begin{aligned} w_+ &= \cos\chi\sin\psi\cosh\vartheta + \sin\chi\cos\psi\cosh\varphi, \\ t_+ &= -\sin\chi\sin\psi\cosh\vartheta + \cos\chi\cos\psi\cosh\varphi, \\ w_- &= \cos\chi\sin\psi\sinh\vartheta + \sin\chi\cos\psi\sinh\varphi, \\ t_- &= -\sin\chi\sin\psi\sinh\vartheta + \cos\chi\cos\psi\sinh\varphi. \end{aligned} \tag{A3}$$

We can directly confirm that the required unitarity relations in Eqs. (35) are always satisfied by arbitrary values of four parameters, ψ, ϑ, φ, and χ.

Eliminating four nondiagonal combinations $\alpha^\dagger\alpha^\dagger + \alpha\alpha$, $\beta^\dagger\beta^\dagger + \beta\beta$, $\alpha^\dagger\beta^\dagger + \beta^\dagger\alpha^\dagger + \alpha\beta + \beta\alpha$, and $\alpha^\dagger\beta + \beta^\dagger\alpha + \alpha\beta^\dagger + \beta\alpha^\dagger$ appearing in H_2, we derive a set of four equations to determine four parameters, i.e.,

$$\begin{aligned} &\tanh 2\vartheta\{A + C + (A - C)\cos 2\chi - 2G\sin 2\chi\} \\ &\quad + B + D + (B - D)\cos 2\chi - 2F\sin 2\chi = 0, \end{aligned} \tag{A4}$$

$$\begin{aligned} &\tanh 2\varphi\{A + C - (A - C)\cos 2\chi + 2G\sin 2\chi\} \\ &\quad + B + D - (B - D)\cos 2\chi + 2F\sin 2\chi = 0, \end{aligned} \tag{A5}$$

$$\begin{aligned} &\tanh(\vartheta + \varphi)\{(A - C)\sin 2\chi + 2G\cos 2\chi\} \\ &\quad + (B - D)\sin 2\chi + 2F\cos 2\chi = 0, \end{aligned} \tag{A6}$$

where A, B, C, D, F, and G are defined in Eqs. (25) in the text. We eliminate ϑ and φ from the above three equations to derive an equation determining 2χ. First, we solve this equation, and subsequently we determine $\tanh 2\vartheta$ and $\tanh 2\varphi$. Then, $\tan 2\psi$ is obtained from the fourth equation:

$$\begin{aligned} &\tan 2\psi\left[\frac{1}{\cosh 2\vartheta}\{A + C + (A - C)\cos 2\chi - 2G\sin 2\chi\}\right. \\ &\left. - \frac{1}{\cosh 2\varphi}\{A + C - (A - C)\cos 2\chi + 2G\sin 2\chi\}\right] \\ &+ \frac{2}{\cosh(\vartheta + \varphi)}\{(A - C)\sin 2\chi + 2G\cos 2\chi\} = 0. \end{aligned} \tag{A7}$$

Practically, χ is numerically calculated in the region of $0 \leqslant \chi \leqslant \pi/2$, and then ψ, ϑ, and φ are obtained. Solving these equations is equivalent to searching for the roots of an algebraic equation of fourth order, as has been done in the text.

APPENDIX B: SIX COEFFICIENTS IN H_4

By introducing the notation

$$\begin{aligned} &C_1 = -\frac{1}{2}A_{yzx}, \quad C_2 = -\frac{1}{2}a_{yzx}, \quad C_3 = -\frac{1}{2}A_{yz}, \\ &C_4 = -\frac{1}{2}a_{yz}, \quad C_5 = -2A_x, \\ &C_6 = -\frac{1}{2}\sqrt{\frac{j}{I}}(A_y + A_z),\ C_7 = -\frac{1}{2}\sqrt{\frac{I}{j}}(A_y + A_z), \\ &C_8 = -\frac{1}{2}\sqrt{\frac{j}{I}}A_{yz},\ C_9 = -\frac{1}{2}\sqrt{\frac{I}{j}}A_{yz}, \end{aligned} \tag{B1}$$

we express the six coefficient C's, which appear in relation (39), in terms of the boson transformation coefficients $u_\pm$, $v_\pm$, $w_\pm$, and $t_\pm$ as follows.

(i) The coefficient of constant term C_0 is given by

$$\begin{aligned} C_0 = {} & C_1\{(u_+u_- + w_+w_-)^2 + 2(u_-^2 + w_-^2)^2\} \\ & + C_2\{(v_+v_- + t_+t_-)^2 + 2(v_-^2 + t_-^2)^2\} \\ & + 3C_3(u_+u_- + w_+w_-)(u_-^2 + w_-^2) \\ & + 3C_4(v_+v_- + t_+t_-)(v_-^2 + t_-^2) + C_5\{(u_-^2 + w_-^2) \\ & \times (v_-^2 + t_-^2) + (u_+w_- + u_-w_+)(v_+t_- + v_-t_+) \\ & + 2u_+u_-v_+v_- + 2w_+w_-t_+t_-\} + C_6\{(u_+u_- + w_+w_-) \\ & \times (u_-v_- + w_-t_-) + 2(u_-^2 + w_-^2)(u_-v_+ + w_-t_+)\} \\ & + C_7\{(v_+v_- + t_+t_-)(u_-v_- + w_-t_-) + 2(v_-^2 + t_-^2) \\ & \times (u_+v_- + w_+t_-)\} + C_8\{(u_+u_- + w_+w_-) \\ & \times (u_+v_- + w_+t_-) + 2(u_-^2 + w_-^2)(u_-v_- + w_-t_-)\} \\ & + C_9\{(v_+v_- + t_+t_-)(u_-v_+ + w_-t_+) \\ & + 2(v_-^2 + t_-^2)(u_-v_- + w_-t_-)\}. \end{aligned} \tag{B2}$$

(ii) The coefficient of the $\hat{n}_\alpha$ term is given by

$$\begin{aligned} C_\alpha = {} & C_1\{3u_-^2(u_+^2 + u_-^2) - u_+^2(u_+^2 - u_-^2) + 4u_+u_-w_+w_- \\ & + 4w_-^2(u_+^2 + u_-^2)\} + C_2\{3v_-^2(v_+^2 + v_-^2) \\ & - v_+^2(v_+^2 - v_-^2) + 4v_+v_-t_+t_- + 4t_-^2(v_+^2 + v_-^2)\} \\ & + 3C_3\{w_+w_-(u_+^2 + u_-^2) + 2u_+u_-(u_-^2 + w_-^2)\} \\ & + 3C_4\{t_+t_-(v_+^2 + v_-^2) + 2v_+v_-(v_-^2 + t_-^2)\} \\ & + C_5\{(u_+^2 + u_-^2)(v_-^2 + t_-^2) + (v_+^2 + v_-^2)(u_-^2 + w_-^2) \\ & + 2u_+u_-v_+v_- + (u_+w_- + u_-w_+)(v_+t_- + v_-t_+) \\ & + (u_+w_+ + u_-w_-)(v_+t_+ + v_-t_-)\} \\ & + C_6\{u_+^2(u_-v_+ - u_+v_-) + 3u_-^2(u_+v_- + u_-v_+) \\ & + w_+w_-(u_+v_+ + u_-v_-) + 2w_-^2(u_+v_- + u_-v_+) \\ & + 2w_-t_+(u_+^2 + u_-^2) + 2u_+u_-w_-t_-\} \\ & + C_7\{v_+^2(u_+v_- - u_-v_+) + 3v_-^2(u_+v_- + u_-v_+) \\ & + t_+t_-(u_+v_+ + u_-v_-) + 2t_-^2(u_+v_- + u_-v_+) \\ & + 2w_+t_-(v_+^2 + v_-^2) + 2v_+v_-w_-t_-\} \\ & + C_8\{u_+v_+(u_-^2 - u_+^2) + 3u_-v_-(u_+^2 + u_-^2) \\ & + 2u_+u_-w_+t_- + 2w_-t_-(u_+^2 + u_-^2) \\ & + 2w_-^2(u_+v_+ + u_-v_-) + w_+w_-(u_+v_- + u_-v_+)\} \\ & + C_9\{u_+v_+(v_-^2 - v_+^2) + 3u_-v_-(v_+^2 + v_-^2) \\ & + 2v_+v_-w_+t_- + 2w_-t_-(v_+^2 + v_-^2) \\ & + 2t_-^2(u_+v_+ + u_-v_-) + t_+t_-(u_+v_- + u_-v_+)\}. \end{aligned} \tag{B3}$$

(iii) The coefficient of the $\hat{n}_\beta$ term is given by

$$\begin{aligned} C_\beta = {} & C_1\{3w_-^2(w_+^2 + w_-^2) - w_+^2(w_+^2 - w_-^2) + 4u_+u_-w_+w_- \\ & + 4u_-^2(w_+^2 + w_-^2)\} + C_2\{3t_-^2(t_+^2 + t_-^2) - t_+^2(t_+^2 - t_-^2) \\ & + 4v_+v_-t_+t_- + 4v_-^2(t_+^2 + t_-^2)\} + 3C_3\{u_+u_-(w_+^2 + w_-^2) \\ & + 2w_+w_-(u_-^2 + w_-^2)\} + 3C_4\{v_+v_-(t_+^2 + t_-^2) \end{aligned}$$

$$
\begin{aligned}
&+2t_+t_-(v_-^2+t_-^2)\}+C_5\{(w_+^2+w_-^2)(v_-^2+t_-^2)\\
&+(t_+^2+t_-^2)(u_-^2+w_-^2)+2w_+w_-t_+t_-\\
&+(u_+w_-+u_-w_+)(v_+t_-+v_-t_+)\\
&+(u_+w_++u_-w_-)(v_+t_++v_-t_-)\}\\
&+C_6\{w_+^2(w_-t_+-w_+t_-)+3w_-^2(w_+t_-+w_-t_+)\\
&+u_+u_-(w_+t_++w_-t_-)+2u_-^2(w_+t_-+w_-t_+)\\
&+2u_-v_+(w_+^2+w_-^2)+2u_-v_-w_+w_-\}\\
&+C_7\{t_+^2(w_+t_--w_-t_+)+3t_-^2(w_+t_-+w_-t_+)\\
&+v_+v_-(w_+t_++w_-t_-)+2v_-^2(w_+t_-+w_-t_+)\\
&+2u_+v_-(t_+^2+t_-^2)+2u_-v_-t_+t_-\}\\
&+C_8\{w_+t_+(w_-^2-w_+^2)+3w_-t_-(w_+^2+w_-^2)\\
&+2w_+w_-u_+v_-+2u_-v_-(w_+^2+w_-^2)\\
&+2u_-^2(w_+t_++w_-t_-)+u_+u_-(w_+t_-+w_-t_+)\}\\
&+C_9\{w_+t_+(t_-^2-t_+^2)+3w_-t_-(t_+^2+t_-^2)+2t_+t_-u_-v_+\\
&+2u_-v_-(t_+^2+t_-^2)+2v_-^2(w_+t_++w_-t_-)\\
&+v_+v_-(w_+t_-+w_-t_+)\}. \qquad \text{(B4)}
\end{aligned}
$$

(iv) The coefficient of the $\hat{n}_\alpha^2$ term is given by

$$
\begin{aligned}
C_{\alpha\alpha}=&\,C_1\{(u_+^2+u_-^2)^2+2u_+^2u_-^2\}+C_2\{(v_+^2+v_-^2)^2\\
&+2v_+^2v_-^2\}+3C_3u_+u_-(u_+^2+u_-^2)\\
&+3C_4v_+v_-(v_+^2+v_-^2)+C_5\{(u_+^2+u_-^2)(v_+^2+v_-^2)\\
&+2u_+u_-v_+v_-\}+C_6\{(u_+v_-+u_-v_+)(u_+^2+u_-^2)\\
&+u_+u_-(u_+v_++u_-v_-)\}+C_7\{(u_+v_-+u_-v_+)\\
&\times(v_+^2+v_-^2)+v_+v_-(u_+v_++u_-v_-)\}\\
&+C_8\{(u_+^2+u_-^2)(u_+v_++u_-v_-)\\
&+u_+u_-(u_+v_-+u_-v_+)\}+C_9\{(v_+^2+v_-^2)\\
&\times(u_+v_++u_-v_-)+v_+v_-(u_-v_++u_+v_-)\}. \qquad \text{(B5)}
\end{aligned}
$$

(v) The coefficient of the $\hat{n}_\beta^2$ term is given by

$$
\begin{aligned}
C_{\beta\beta}=&\,C_1\{(w_+^2+w_-^2)^2+2w_+^2w_-^2\}+C_2\{(t_+^2+t_-^2)^2\\
&+2t_+^2t_-^2\}+3C_3w_+w_-(w_+^2+w_-^2)+3C_4t_+t_-\\
&\times(t_+^2+t_-^2)+C_5\{(w_+^2+w_-^2)(t_+^2+t_-^2)\\
&+2w_+w_-t_+t_-\}+C_6\{(w_+t_-+w_-t_+)(w_+^2+w_-^2)\\
&+w_+w_-(w_+t_++w_-t_-)\}+C_7\{(w_+t_-+w_-t_+)\\
&\times(t_+^2+t_-^2)+t_+t_-(w_+t_++w_-t_-)\}\\
&+C_8\{(w_+t_++w_-t_-)(w_+^2+w_-^2)\\
&+w_+w_-(w_+t_-+w_-t_+)\}+C_9\{(w_+t_++w_-t_-)\\
&\times(t_+^2+t_-^2)+t_+t_-(w_+t_-+w_-t_+)\}. \qquad \text{(B6)}
\end{aligned}
$$

(vi) The coefficient of the $\hat{n}_\alpha\hat{n}_\beta$ term is given by

$$
\begin{aligned}
C_{\alpha\beta}=&\,4C_1\{(u_+^2+u_-^2)(w_+^2+w_-^2)+2u_+u_-w_+w_-\}\\
&+4C_2\{(v_+^2+v_-^2)(t_+^2+t_-^2)+2v_+v_-t_+t_-\}\\
&+6C_3\{u_+u_-(w_+^2+w_-^2)+w_+w_-(u_+^2+u_-^2)\}\\
&+6C_4\{v_+v_-(t_+^2+t_-^2)+t_+t_-(v_+^2+v_-^2)\}\\
&+C_5\{(u_+^2+u_-^2)(t_+^2+t_-^2)+(v_+^2+v_-^2)(w_+^2+w_-^2)\\
&+2(u_+w_-+u_-w_+)(v_+t_-+v_-t_+)\\
&+2(u_+w_++u_-w_-)(v_+t_++v_-t_-)\}\\
&+2C_6\{(u_+^2+u_-^2)(w_+t_-+w_-t_+)+(w_+^2+w_-^2)\\
&\times(u_+v_-+u_-v_+)+w_+w_-(u_+v_++u_-v_-)\\
&+u_+u_-(w_+t_++w_-t_-)\}+2C_7\{(v_+^2+v_-^2)\\
&\times(w_+t_-+w_-t_+)+(t_+^2+t_-^2)(u_+v_-+u_-v_+)\\
&+t_+t_-(u_+v_++u_-v_-)+v_+v_-(w_+t_++w_-t_-)\}\\
&+2C_8\{(u_+^2+u_-^2)(w_+t_++w_-t_-)+(w_+^2+w_-^2)\\
&\times(u_+v_++u_-v_-)+u_+u_-(w_+t_-+w_-t_+)\\
&+w_+w_-(u_+v_-+u_-v_+)\}+2C_9\{(v_+^2+v_-^2)\\
&\times(w_+t_++w_-t_-)+(t_+^2+t_-^2)(u_+v_++u_-v_-)\\
&+v_+v_-(w_+t_-+w_-t_+)+t_+t_-(u_+v_-+u_-v_+)\}. \qquad \text{(B7)}
\end{aligned}
$$

APPENDIX C: THE COEFFICIENTS $G^{Ij}_{n_a,n_b;n_\alpha,n_\beta}$

The general Bogoliubov transformation connecting HP boson operators $(\hat{a},\hat{b},\hat{a}^\dagger,\hat{b}^\dagger)$ to quasiboson operators $(\alpha,\beta,\alpha^\dagger,\beta^\dagger)$ is rewritten as

$$
\begin{pmatrix}\alpha_\mu\\ \alpha_\mu^\dagger\end{pmatrix}\equiv\begin{bmatrix}K & N\\ M & L\end{bmatrix}\begin{pmatrix}\hat{a}_\mu\\ \hat{a}_\mu^\dagger\end{pmatrix}, \qquad \text{(C1)}
$$

where the subscript $\mu\,(=1,2)$ is used to discriminate two kinds of bosons as $\hat{a}_1\equiv\hat{a},\hat{a}_2\equiv\hat{b},\alpha_1\equiv\alpha$ and $\alpha_2\equiv\beta$. Numbers of HP bosons are limited to $0\leqslant n_a\leqslant 2I$ and $0\leqslant n_b\leqslant 2j$. To guarantee the equivalence of two Fock spaces, the quasiboson Fock space is also truncated by $0\leqslant n_\alpha\leqslant 2I$ and $0\leqslant n_\beta\leqslant 2j$, and then the 2×2 matrices in Eq. (C1), $K(=L)$ and $M(=N)$, are square and nonsingular, i.e., $\det K\neq 0$. Correspondingly, the state vectors are properly normalized, though we have not been concerned with the practice of this normalization in the present paper. By the generalized Wick theorem [17] as presented in Eq. (51) in the text, any matrix element of the form ${}_a\langle 0|a_1a_2\ldots a_m\alpha_{m+1}^\dagger\alpha_{m+2}^\dagger\ldots\alpha_{2n}^\dagger|0\rangle_\alpha$ can be reduced to a summation of the products of three kinds of matrix element as building blocks:

$$
\begin{aligned}
A_{\mu\nu}\equiv&\,\frac{{}_a\langle 0|\alpha_\mu^\dagger\alpha_\nu^\dagger|0\rangle_\alpha}{{}_a\langle 0|0\rangle_\alpha}=(MK^{-1})_{\mu\nu}\\
=&-\begin{bmatrix}\cos^2\psi\tanh\vartheta+\sin^2\psi\tanh\varphi & \cos\psi\sin\psi(\tanh\vartheta-\tanh\varphi)\\ \cos\psi\sin\psi(\tanh\vartheta-\tanh\varphi) & \sin^2\psi\tanh\vartheta+\cos^2\psi\tanh\varphi\end{bmatrix}_{\mu\nu}, \qquad \text{(C2)}
\end{aligned}
$$

$$
\begin{aligned}
B_{\mu\nu}\equiv&\,\frac{{}_a\langle 0|a_\mu a_\nu|0\rangle_\alpha}{{}_a\langle 0|0\rangle_\alpha}=-(K^{-1}N)_{\mu\nu}\\
=&\begin{bmatrix}\cos^2\chi\tanh\vartheta+\sin^2\chi\tanh\varphi & -\cos\chi\sin\chi(\tanh\vartheta-\tanh\varphi)\\ -\cos\chi\sin\chi(\tanh\vartheta-\tanh\varphi) & \sin^2\chi\tanh\vartheta+\cos^2\chi\tanh\varphi\end{bmatrix}_{\mu\nu}, \qquad \text{(C3)}
\end{aligned}
$$

$$C_{\mu\nu} \equiv \frac{{}_a\langle 0|a_\mu \alpha_\nu^\dagger|0\rangle_\alpha}{{}_a\langle 0|0\rangle_\alpha} = (K^{-1})_{\mu\nu}$$
$$= \frac{1}{\cosh\vartheta\cosh\varphi} \times \begin{bmatrix} -\sin\psi\sin\chi\cosh\vartheta + \cos\psi\cos\chi\cosh\varphi & \cos\psi\sin\chi\cosh\vartheta + \sin\psi\cos\chi\cosh\varphi \\ -\sin\psi\cos\chi\cosh\vartheta - \cos\psi\sin\chi\cosh\varphi & \cos\psi\cos\chi\cosh\vartheta - \sin\psi\sin\chi\cosh\varphi \end{bmatrix}_{\mu\nu}, \tag{C4}$$

with

$${}_a\langle 0|0\rangle_\alpha = \frac{1}{\sqrt{\det K}} = \frac{1}{\sqrt{\cosh\vartheta\cosh\varphi}}. \tag{C5}$$

By the Wick theorem in Eq. (51), $G^{Ij}_{n_a,n_b;n_\alpha,n_\beta}$ defined in Eq. (54) is reduced to a sum of the products among the matrix elements of $A_{\mu\nu}$, $B_{\mu\nu}$, and $C_{\mu\nu}$ defined in Eqs. (C2), (C3), and (C4). Here we list a few examples of G's for some simple cases, which appear in Sec. IV:

$$G_{0000} = {}_a\langle 0|0\rangle_\alpha = \frac{1}{(\cosh\vartheta\cosh\varphi)^{1/2}}, \tag{C6}$$

$$G_{1010} = G_{0000}C_{11} = -\frac{\sin\psi\sin\chi\cosh\vartheta - \cos\psi\cos\chi\cosh\varphi}{(\cosh\vartheta\cosh\varphi)^{3/2}}, \tag{C7}$$

$$G_{1001} = G_{0000}C_{12} = \frac{\cos\psi\sin\chi\cosh\vartheta + \sin\psi\cos\chi\cosh\varphi}{(\cosh\vartheta\cosh\varphi)^{3/2}}, \tag{C8}$$

$$G_{0110} = G_{0000}C_{21} = -\frac{\sin\psi\cos\chi\cosh\vartheta + \cos\psi\sin\chi\cosh\varphi}{(\cosh\vartheta\cosh\varphi)^{3/2}}, \tag{C9}$$

$$G_{0101} = G_{0000}C_{22} = \frac{\cos\psi\cos\chi\cosh\vartheta - \sin\psi\sin\chi\cosh\varphi}{(\cosh\vartheta\cosh\varphi)^{3/2}}. \tag{C10}$$

In the above expressions, $G_{n_an_bn_\alpha n_\beta}$ is an abbreviation of $G^{Ij}_{n_a,n_b;n_\alpha,n_\beta}$.

The next-order matrices with $n_a + n_b - n_\alpha - n_\beta = 2$ are calculated by use of the matrix elements of $B_{\mu\nu}$ and $C_{\mu\nu}$ as follows:

$$G_{2000} = \frac{G_{0000}}{(2!)^{1/2}}B_{11},$$
$$G_{1100} = G_{0000}B_{12},$$
$$G_{0200} = \frac{G_{0000}}{(2!)^{1/2}}B_{22},$$
$$G_{3010} = \frac{3G_{0000}}{(3!)^{1/2}}B_{11}C_{11},$$
$$G_{3001} = \frac{3G_{0000}}{(3!)^{1/2}}B_{11}C_{12},$$
$$G_{2110} = \frac{G_{0000}}{(2!)^{1/2}}(B_{11}C_{21} + 2C_{11}B_{12}),$$
$$G_{2101} = \frac{G_{0000}}{(2!)^{1/2}}(B_{11}C_{22} + 2B_{12}C_{12}). \tag{C11}$$

When $\vartheta = \varphi = \psi = \chi = 0$, $G_{n_an_bn_\alpha n_\beta} = 1$, if $n_a = n_\alpha$ and $n_b = n_\beta$; $G_{n_an_bn_\alpha n_\beta} = 0$, otherwise.

[1] S. W. Ødegård *et al.*, Phys. Rev. Lett. **86**, 5866 (2001).
[2] D. R. Jensen *et al.*, Phys. Rev. Lett. **89**, 142503 (2002).
[3] D. R. Jensen *et al.*, Nucl. Phys. **A703**, 3 (2002).
[4] A. Görgen *et al.*, Phys. Rev. C **69**, 031301(R) (2004).
[5] G. Schönwaßer *et al.*, Phys. Lett. **B552**, 9 (2003).
[6] H. Amro *et al.*, Phys. Lett. **B553**, 197 (2003).
[7] A. Bohr and B. R. Mottelson, *Nuclear Structure* (Benjamin, Reading, MA, 1975), Vol. II, Chap. 4.
[8] I. Hamamoto, Phys. Rev. C **65**, 044305 (2002).
[9] I. Hamamoto and G. B. Hagemann, Phys. Rev. C **67**, 014319 (2003).
[10] K. Tanabe and K. Sugawara-Tanabe, Phys. Lett. **B34**, 575 (1971).
[11] A. Bohr, Mat. Fys. Medd. Dan. Vidensk. Selsk. **26**, no. 14 (1952).
[12] K. Tanabe and K. Sugawara-Tanabe, Phys. Rev. C **14**, 1963 (1976).
[13] C. Bloch and A. Messiah, Nucl. Phys. **39**, 95 (1962).
[14] J. Mayer ter Vehn, S. F. Stephens, and R. M. Diamond, Phys. Rev. Lett. **32**, 1383 (1974).
[15] K. Tanabe, J. Math. Phys. **14**, 618 (1973).
[16] K. Sugawara-Tanabe and K. Tanabe, Nucl. Phys. **A208**, 317 (1973).
[17] K. Tanabe, K. Enami, and N. Yoshinaga, Phys. Rev. C **59**, 2494 (1999).
[18] D. R. Jensen *et al.*, Eur. Phys. J. A **19**, 173 (2004).